University of Stuttgart
Institute of Geodesy

Assessing the performance of different classification methods to detect inland surface water extent

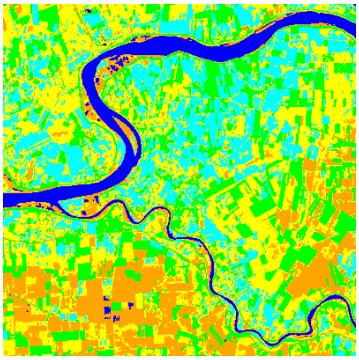

Bachelor Thesis

Geodäsie und Geoinformatik

University of Stuttgart

Alexander Walton

Stuttgart, August 2015

Supervisors: Prof. Dr.-Ing. Nico Sneeuw
University of Stuttgart

Dr.-Ing. Mohammad J. Tourian
University of Stuttgart

M.Sc. Omid Elmi
University of Stuttgart

Erklärung der Urheberschaft

Ich erkläre hiermit an Eides statt, dass ich die vorliegende Arbeit ohne Hilfe Dritter und ohne Benutzung anderer als der angegebenen Hilfsmittel angefertigt habe; die aus fremden Quellen direkt oder indirekt übernommenen Gedanken sind als solche kenntlich gemacht. Die Arbeit wurde bisher in gleicher oder ähnlicher Form in keiner anderen Prüfungsbehörde vorgelegt und auch noch nicht veröffentlicht.

Ort, Datum Unterschrift

Abstract

In recent decades, political as well as environmental conflicts about the Earth's water resources became a significant issue with constantly growing importance all over the world. These issues include flooding as well as drying shrinkage of seas and rivers. In order to estimate the dimension of these impacts, reliable frequent observation of the surface water over a long period of time is essential.

By making use of the special spectral reflectance properties of water, especially in higher spectral ranges, it is possible to distinguish between water and other surface materials and create thematic maps using different classification methods. These methods can be based on *supervised* algorithms which make use of training data to classify an image. On the other hand they can be automatized computing algorithms which assign pixels to a class without any prior knowledge. The latter are referred as *unsupervised* methods.

Assessing the performance of these various methods will be task of this thesis. Here in this study four satellite images of Landsat 7 are selected for our case study. The images show the region around the Po River in northern Italy. The valley alongside the river is one of the strongest economic and agricultural region in Italy but it also suffers from regular flooding, especially in the delta region around Ferrara close to the Adriatic Sea.

The different classification methods are implemented in the software ENVI which is commonly used by remote sensing professionals to process and analyse geospatial imagery.

To make a statement about the accuracy of the single classification methods every classifier undergoes a few essential steps: A binary water mask is created in which the river width is measured at two selected gauge spots. At these spots precise in-field measurements were applied regularly in recent years and the results serve as reference values for a comparison in between the classification methods.

In general the supervised methods performed better than the unsupervised methods. The best performance is approached by the mahalanobis distance classification which is based on probability statistics with consistent covariances. This way the pixels can be classified by calculating their minimum euclidean distance in spectral space.

The results of this study are limited by the low resolution of 30 m which does not leave vast room for interpretation. More reliable results could be achieved by measuring effective widths alongside the river and apply an area-wise comparison. However approximate estimates about the performance of the different classification methods and good first impressions of the advantages and disadvantages are given.

Contents

List of Figures

List of Tables

Chapter 1

Introduction

1.1 Energy Sources and Wavelength Ranges

In order to construct an image from the Earth's surface, reflected energy is measured using a sensor mounted on an aircraft or spacecraft platform. The process from collecting data to the resolution of an image is shown in a simplified view in Figure 1.1. The most obvious source of energy would be reflected sunlight, so that the later formed image is in many ways similar to the view we would have of the Earth's surface from an aircraft [8]. Such a sensor is referred to as a *passive* sensor. Alternatively the upwelling energy could also be radiated from the Earth itself or provided by an *active* sensor, such as a laser or radar. In remote sensing wavelength ranges far beyond the range of the human vision are used. Short-, long-waved infrared and sometimes even ultraviolet wavelength ranges are established.

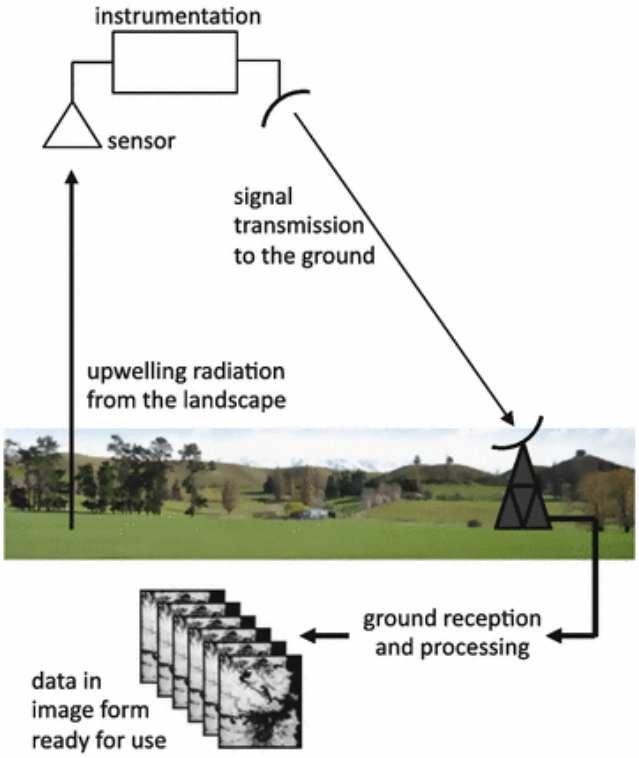

Figure 1.1: *Signal flow in a remote sensing system [8]*

As long as there is any source of energy available, almost every wavelength could be used to measure the characteristics of the Earth's surface. However, the wavelengths used in remote sensing, particularly when imaging from spacecraft altitudes, are limited to a so called *atmospheric window* [8]. Energy at some wavelengths is absorbed by the molecular constituents in the Earth's atmosphere, such as ozone, water vapour and carbon dioxide. The *atmospheric window* describes an area in which there is little or no atmospheric absorption. As shown in Figure 1.2 there are various amounts of windows in the visible and infrared regions and radio wavelengths even possess almost complete transparency of the atmosphere.

Based on these significant absorption properties, optical remote sensing systems record data from the visible through to near and mid-infrared range, which covers approximately 0.4–2.5 µm [8].

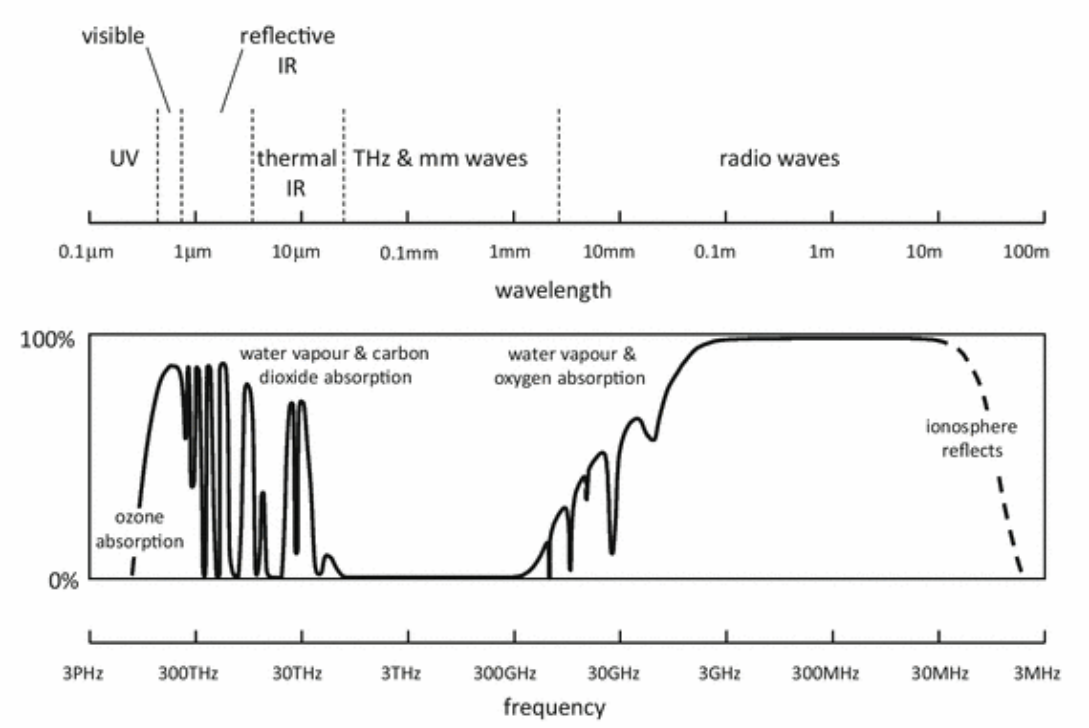

Figure 1.2: *The electromagnetic spectrum and the transmittance of the earth's atmosphere [8]*

1.2 Spectral reflectance properties

Earth surface objects absorb or reflect sunlight in different ways. The reflectance properties depend on the materials physical and chemical state, which is why most of them have quite complex absorption characteristics. The differences can be visualised in so called spectral reflectance curves as a function of wavelengths. Figure 1.3 shows a typical spectral reflectance curve for three basic type of Earth features: green vegetation, dry bare soil and clear water.

The spectral reflectance properties of water are characterized by a high to almost total absorption at near infrared and beyond. Using linear combinations of different bands with their respective wavelength ranges, water bodies or water containing objects can easily be detected

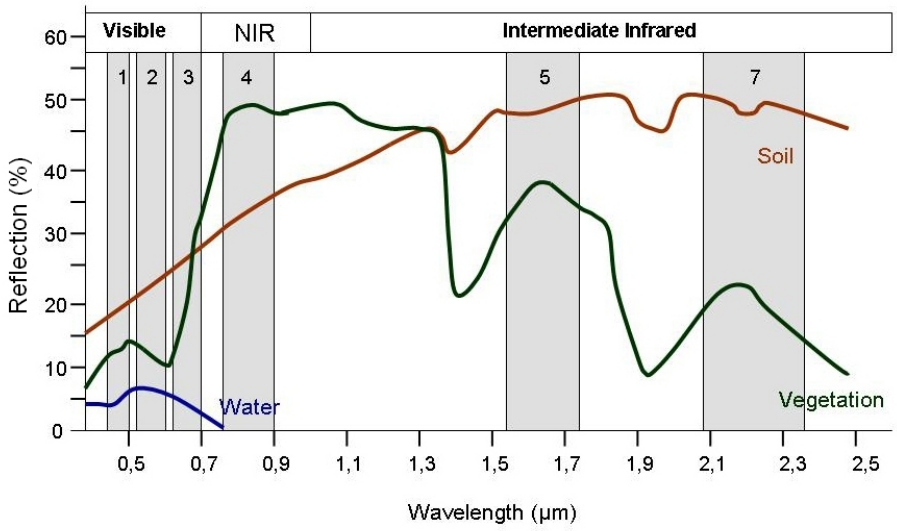

Figure 1.3: *Spectral signature of soil, vegetation and water with spectral bands of Landsat 7 [10]*

and delineated. We can distinguish between turbid water and clear water because of its higher reflectance in the visible region and in a similar manner we can detect oil spills or industrial wasted water or even algae colonies by making use of its high concentration of chlorophyll. Chlorophyll strongly absorbs light at wavelengths in the blue and red ranges and shows high reflection properties in the green region, therefore healthy vegetation appears in colours of green in the human vision. The reflection in infrared ranges varies amongst different plant species, with which a distinction between the species can be accomplished [10].

1.3 Satellite Imagery Missions

Optical and synthetic aperture radar (SAR) satellite imagery missions are capable of detecting inland surface water extent [1]. The Landsat Multispectral Scanner System (MSS) launched in 1972 began the modern era of land remote sensing from space. It was equipped with a 80 m spatial resolution sensor with 4 spectral bands, each about 0.1 µm wide. Today operational satellite systems sample nearly all available parts of the electromagnetic spectrum with dozens of spectral bands and spatial resolutions of better than 1 m [9]. The essential differences in the several satellite imagery missions are characterized by the number and coverage of the spectral bands, the spatial resolution, the coverage area and the temporal resolution. SAR imaging systems are additionally classified according to the combination of frequency bands but since this study is limited to optical images the SAR missions will not be of any further interest. Figure 1.4 presents different optic and SAR missions.

The first remote sensing satellite capable of water body and wetland monitoring was the advanced very high resolution radiometer (AVHRR) and it is available since 1980. Its pixel size of approximately 1 x 1 km has been improved over the year to reach spatial resolutions in range of metres. For example one of the most recent satellite missions is the Landsat 8 mission with a

spatial resolution of 30 m. MODIS is capable of scanning the Earth's surface in only two days with a spatial resolution of 250 m [1].

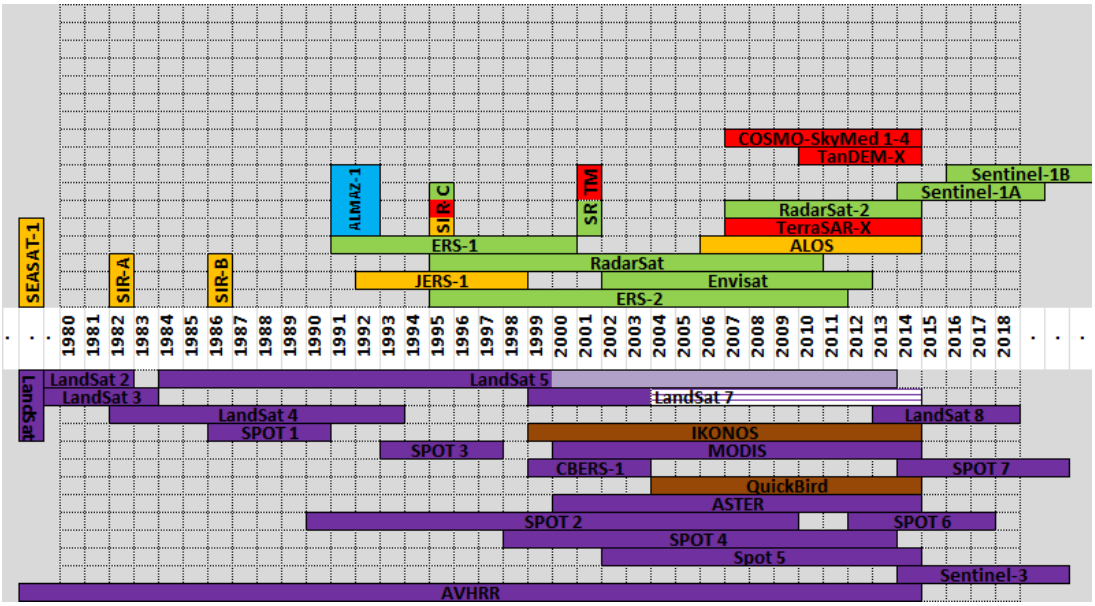

Figure 1.4: *Different optic and SAR missions [1]*

Table 1.1 gives us a brief summary of various sensor properties. If the resolution would be the most important parameter, Worldview and Geoeye would be the best choices available. However, these sensors also differ in their number of spectral bands and the spectral range. Airborne sensors provide the widest spectral range, followed by Landsat, SPOT and IRS. Airborne sensors suffer from range and time, therefore Landsat is the optimal choice if the spectral and operational ranges are considered [11]. Landsat 7 data shows a great availability and is free of charge. For those reasons Landsat 7 imagery is used in this study. Therefore, here we discuss further about the properties of Landsat 7.

Table 1.1: *Summary of sensor properties*

Sensor	Spatial resolution [m]	Spectral range [µm]	Temporal resolution [days]
Landsat 7	15	0.45–2.35	16
SPOT	2.5	0.50–1.75	5
IRS	5	0.50–1.70	5
Ikonos	1	0.45–0.85	3
Quickbird	0.61	0.45–0.90	3
Worldview	0.46	0.40–1.04	1.1
ALOS	2.5	0.42–0.89	2
Geoeye	0.41	0.45–0.90	3
Airborne	1–25	0.42–14.00	N/A

1.4 Landsat 7

Landsat 7 is an Earth observing satellite launched in 1999. Back then no other system could match the Landsat's combination of synoptic coverage, high spatial resolution, spectral range and radiometric calibration. Table 1.2 provides detailed information about the orbital parameters. Unlike its predecessors, Landsat 7 is still active today. The very first Landsat satellite was launched in 1972 and terminated in 1978. Landsat 5 was terminated in 2013 after a duration of almost 30 years. Landsat 6 failed to reach the orbit in 1993 so a lot of hope was build on the Landsat 7 mission.

The system was supposed to insure continuity of Thematic Type data into the next century, but on May 31, 2003 the Scan Line Corrector (SLC) in the sensor failed. The purpose of the SLC was to compensate forward motion (along-track) of the spacecraft so that the resulting scans are aligned parallel to each other. This was permitted by a pair of small mirrors that rotate about an axis in tandem with the motion of the main scan mirror. Without an operation of SLC the scanner traces a zig-zac pattern resulting in duplicated areas in the image. Nevertheless the satellite is still capable of acquiring useful image data with the SLC turned off since the distortions are most pronounced along the edge and gradually diminished towards the center of the scene. An estimated 22% of any given scene is lost because of the SLC failure [13].

Landsat 7 has catalogued the world's land mass into 57.784 scenes, each 183 km wide by 170 km long. It produces approximately 3.8 gigabytes of data for each scene [5].

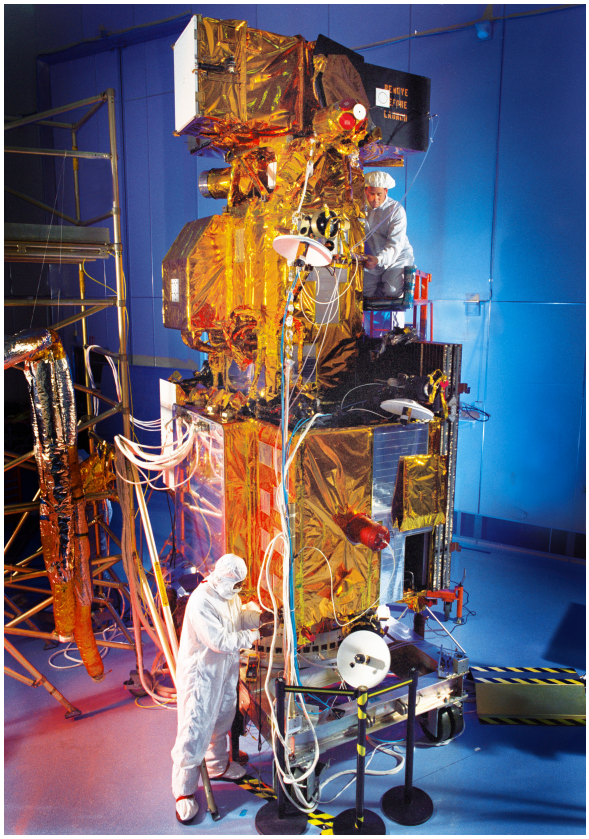

Figure 1.5: *The Landsat 7 satellite in the cleanroom prior to launch [4]*

Table 1.2: *Landsat 7 details*

Launch date	April 15, 1999
Sensor	ETM+
Altitude	705 km
Inclination	98.2 °
Orbit	polar, sun-synchronous
Equational Crossing Time	10 AM
Period of Revolution	99 minutes → ≈14.5 orbits/day
Repeat Coverage	16 days
Dimensions	4.04 m long, 2.74 m diameter

1.4.1 Primary Instrument: ETM+

The primary instrument on Landsat 7 is the Enhanced Thematic Mapper Plus (ETM+). In comparison with the already successful Thematic Mapper (TM) instruments on Landsat 4 and 5 the ETM+ includes new features that make it a more versatile and efficient instrument for global change studies, land cover monitoring and assessment and large area mapping.

Primarily these new features are

- a panchromatic band with 15 m spatial resolution
- an on-board, full aperture, 5% absolute radiometric calibration
- a thermal infrared channel with 60 m spatial resolution

The ETM+ uses a fixed "whisk-broom", eight-band, multispectral scanner to procure 532 high-resolution images of the Earth's surface per day. It detects spectrally-filtered radiation in visible and near-infrared (VNIR), short-wavelength infrared (SWIR) and long-wavelength infrared (LWIR, "thermal infrared). Table 1.4 shows the resolution and wavelength range of every single spectral band in detail. The high spatial resolution of 15 m without losing any information can be achieved by panchromatic image sharpening with the help of the eighth band [5], [6].

Table 1.3: *ETM+ Technical Specifications*

Sensor type	opto-mechanical
Spatial Resolution	30 m (60 m - thermal, 15 m - pan)
Spectral Range	0.45–12.5 µm
Number of bands	8
Temporal Resolution	16 days
Image size	183 km x 170 km

Table 1.4: *ETM+ Bands*

Band Number	µm	Resolution	Light spectrum
1	0.45–0.515	30 m	Blue
2	0.525–0.605	30 m	Green
3	0.63–0.69	30 m	Red
4	0.75–0.90	30 m	Near Infrared
5	1.55–1.75	30 m	Short-wave Infrared
6	10.4–12.5	60 m	Long-wave Infrared
7	2.09–2.35	30 m	Short-wave Infrared
8	0.52–0.90	15 m	Panchromatic

1.4.2 Landsat 8

On February 11, 2013 Landsat 8 joined the earth observation satellites. It utilizes a two-sensor payload, the Operational Land Imager (OLI) and the Thermal InfraRed Sensor (TIRS), which will collect image data on a total of 11 spectral bands reaching from 0.43 to 12.50 µm. The additional three bands are a deep blue band for coastal and aerosol studies, a shortwave infrared band for cirrus detection and a quality assessment band [12]. A comparison of the spectral bands along with the atmospheric transmission is given in Figure 1.6.

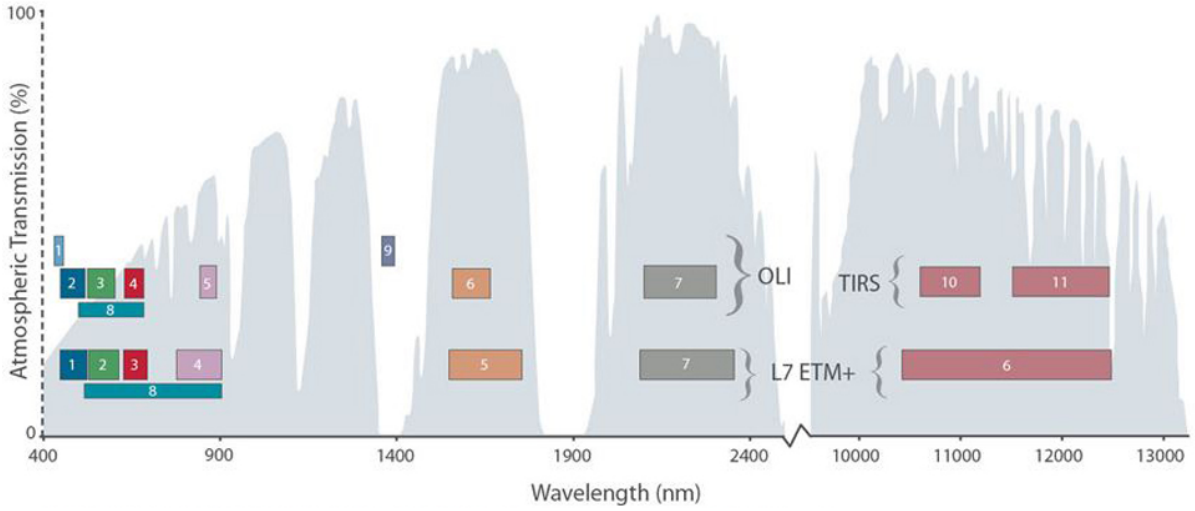

Figure 1.6: *Bandpass wavelengths for Landsat 8 OLI and TIRS sensor, compared to Landsat 7 ETM+ sensor [12]*

1.5 Band sensitivities

Table 1.5 describes how the single bands of Landsat 7 interact to particular materials and how they could be combined to create a first impression of the area intended for closer inspection.

Table 1.5: *Band sensitivities [7], [8]*

Band	Sensitivity / Characteristics	Application
1	Penetration of water bodies Soil and vegetation differences	Detection of cultural features Analysis of land use
2	Reflectance peak of healthy vegetation Sensitive to water turbidity	Separate vegetation from soil
3	Strong absorption of chlorophyll Soil and urban areas highlighted	Discrimination of vegetation
4	High reflectance of chlorophyll Strong absorption of water	Distinguish vegetation varieties Soil-crop and land-water contrast
5	Sensitive to moisture content	Crop draught and plant healthiness studies
6	Sensitive to the Earth's radiation	Measurements of surface temperature
7	Very high water absorption Very high soil reflectance	Separation between land and water Hydrothermal alteration in rocks

1.5.1 Display of remote sensing data

Satellite images are not photographs but pictorial representations of measured data [10]. Combination of certain bands represented in red, green and blue (RGB) now lead to images with more information content compared to solely panchromatic images. In each band, grayscales are assigned respectively to the intensity of the electromagnetic radiation and saved digitally in pixels. Through assigning the three fundamental colours (red, green, blue) to three different bands satellite image composites are produced. Figure 1.7 demonstrates how various band combinations are shown by the Landsat satellite [3].

Figure 1.7a shows a *"True colour"* image. This band combination is used to represent an image in natural colour and therefore best approaches the appearance of the human visual system. Also this solution provides the highest penetration of clear water.
Combination of bands 4,3 and 2 (Figure 1.7b) will result in a *"False colour"* image. Band 4 shows the reflectance peak of chlorophyll, therefore vegetation appears in tones of red. Clear water appears in dark blue to black, thus land-water detection is way easier in this combination.
Another example is the combination of the bands 4,5 and 3 in Figure 1.7c. Band 5 makes use of the water absorption capabilities of water, thus enabling detection of thin water layers. Also variations in soil and rocks can be detected. When a crop has a relative lower moisture content, the reflection from band 5 will be relatively higher, meaning more contribution of green and thus resulting in a more orange colour.
In Figure 1.7d healthy vegetation appears in bright green, therefore this combination can be referred as "natural-like". Band 7 highlights moisture content and is increasingly sensitive to

(a) *"True colour"*
321: combination of red(3) - green(2) - blue(1)

(b) *"False colour"*
432: combination of VNIR(4) - red(3) - green(2)

(c)
453: combination of VNIR(4) - SWIR(5) - red(3)

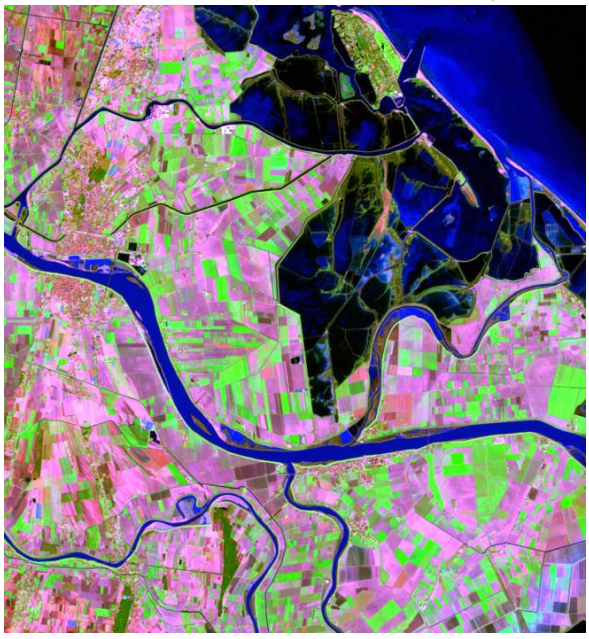

(d)
742: combination of SWIR(7) - VNIR(4) - green(2)

Figure 1.7: *Different combined bands. Depicted is an oceanic region in Italy with urban and fallow as well as vegetated and forestal areas.*

the emissive radiation which enables access to detect heat sources. This combination is often used in desert regions or for geological and wetland studies.

1.6 Vegetation Indices

Other than assigning the three fundamental colours to different bands, mathematical operations applied to the raw data can extract more information. Addition, subtraction and division of the brightness of two or more bands are the most common. For example the *Normalized Difference Vegetation Index* (NDVI) is used to identify the health status of plants, depict phenological changes and other remote sensing measurements [8]. The NDVI is calculated as follows

$$\mathrm{NDVI} = \frac{(\varnothing_{\mathrm{nir}} - \varnothing_{\mathrm{red}})}{(\varnothing_{\mathrm{nir}} + \varnothing_{\mathrm{red}})} \tag{1.1}$$

in which $\varnothing_{\mathrm{nir}}$ is the near infrared brightness of a pixel and $\varnothing_{\mathrm{red}}$ is its visible red brightness. Every Pixel is now represented in values between -1 (no vegetation) and $+1$ (abundant vegetation). For the different classifications in chapter 2 and 3 this index will be used. Two other indices sometimes used are the *Normalized Difference Water Index* (NDWI), which gives an indication of soil moisture

$$\mathrm{NDWI} = \frac{(\varnothing_{\mathrm{green}} - \varnothing_{\mathrm{nir}})}{(\varnothing_{\mathrm{green}} + \varnothing_{\mathrm{nir}})} \tag{1.2}$$

Equivalent $\varnothing_{\mathrm{green}}$ is now the green wavelength brightness of a pixel [8]. In this index, water features values between 0 and $+1$. As a third example, the *Land Surface Water Index* is used to monitor liquid water content in vegetation and soil [8]

$$\mathrm{LSWI} = \frac{(\varnothing_{\mathrm{nir}} - \varnothing_{\mathrm{swir}})}{(\varnothing_{\mathrm{nir}} + \varnothing_{\mathrm{swir}})} \tag{1.3}$$

1.7 Case Study and Data

The study area for this thesis is the Po river in Italy. As visualized in Figure 1.8 it flows 682 km eastward across northern Italy from a spring in the Cottian Alps through a delta projecting into the Adriatic Sea. Very large discharge of the Po leads to heavy flooding in the whole area and consequently into many economic problems. But still the valley is one of the main areas for industry and agriculture thus it appears that reliable frequent observation of the water extent is essential.

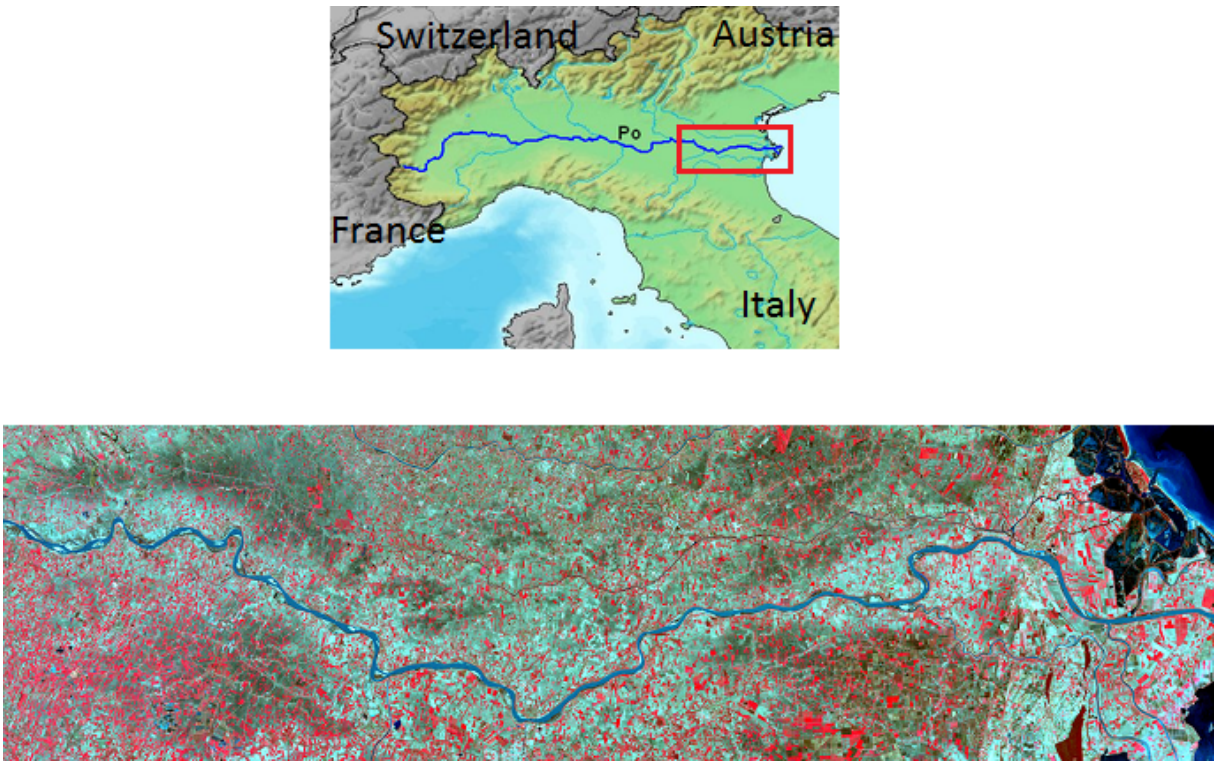

Figure 1.8: *Location of the Po river; Scenery in a negative colour image (band 432)*

A total of four Landsat 7 satellite images are used in this thesis. One for each season of the year 2001. This way different growing seasons and weather influences like clouds or light shade effects will be considered in the single classifications.

1.8 Outline of the Thesis

The physical backgrounds that are required for satellite imagery have been introduced, the interpretation of raw image data will be the task of Chapter 2. There is no single, correct method for analysing digital images, therefore it is important to know the pros and cons of all available options. Various techniques to classify an image and produce maps of land cover, land type and land use will be described in detail in this section. Chapter 3 will illustrate the results in comparison with an in-field surveillance. A concluding discussion will be given in Chapter 4.

Chapter 2

Classification Methods

Digital image classification is a mapping from the spectral measurements acquired by a remote sensing instrument to a set of labels that represent land cover features. Land cover could be agricultural, urban, forested or water-covered types of features. In order to provide a unique label, or theme, for each pixel in the image, different computer processing algorithms are used. This process is called *thematic mapping* and the produced map therefore is referred to as a *thematic map*. Knowing the size of a pixel in the corresponding ground metres, accurate estimates of the area can be calculated [8].

The classification techniques in remote sensing can be categorized in two groups:

- Supervised classification
- Unsupervised classification

2.1 Supervised classification

The major task of the supervised methods is to segment the spectral domain into regions of interest to a particular application. These techniques are mostly used for quantitative analysis and are divided into *soft classification* methods and *hard classification* methods. The difference in these two methods lays in the way they identify and describe the regions in spectral space. Some methods seek a segmentation based on probability distributions while others use simple geometric partition. *Hard classification* generates firm boundaries between classes whereas *soft classification* sometimes leads to spatially overlapped regions [8].

Irrespective of the method chosen, it requires *training pixels* whose class labels are known and which can be used to form *training data* for the desired classifier. A training set can be established using image products formed from the data such as a RGB-image from Section 1.5.1 or the NDVI-resolution from Section 1.6. In spectral domain the training pixels will enclose a common region, the so called *training field*.
The training data can now be used to assess the parameters (*signature*) of a particular classifier and later on label every pixel to one of the predefined classes.

In general the supervised classification follows these essential steps [10]:

- Definition of the different land cover classes
- Classification of suitable training areas
- Employing of the actual classification with a particular algorithm

- Producing a thematic map
- Assessing the accuracy of the final product using a labelled *testing data* set

2.1.1 Maximum Likelihood Classification

The maximum likelihood classification is the most common algorithm used in remote sensing. It uses a probability density function based on *Bayes' classification* rule, meaning that each pixel is assigned to the class that has the highest probability (maximum likelihood). Each pixel is labelled according to the decision rule

$$\mathbf{x} \in \omega_i \quad \text{if} \quad p(\mathbf{x}|\omega_i)p(\omega_i) > p(\mathbf{x}|\omega_j)p(\omega_j) \quad \text{for all} \quad j \neq i \tag{2.1}$$

The classes are represented by $\omega_i, i = 1...M$ where M is the number of classes. $\mathbf{x}$ is a column vector with the brightness values for the pixel in each measurement band, therefore $p(\mathbf{x}|\omega_i)$ describes the chance of finding a pixel at position $\mathbf{x}$ in spectral space from each class ω_i. $p(\omega_i)$ is referred as *prior probability* and describes the probability that pixels from class ω_i appear anywhere in the image.

$p(\mathbf{x})$ can be removed, since it is not class dependant. This leads to the *discriminant function*

$$g_i(\mathbf{x}) = \ln p(\mathbf{x}|\omega_i)p(\omega_i) = \ln p(\mathbf{x}|\omega_i) + \ln p(\omega_i) \tag{2.2}$$

Substitution of (2.2) into (2.1) gives a new decision rule

$$\mathbf{x} \in \omega_i \quad \text{if} \quad g_i(\mathbf{x}) > g_j(\mathbf{x}) \quad \text{for all} \quad j \neq i \tag{2.3}$$

Figure 2.1 shows that the classes of pixels in spectral space are normally distributed (Gaussian distribution) which leads to the *Gaussian maximum likelihood classifier*[1]

$$g_i(\mathbf{x}) = -\ln |\mathbf{C}_i| - (\mathbf{x} - \mathbf{m}_i)^T \mathbf{C}_i^{-1} (\mathbf{x} - \mathbf{m}_i) \tag{2.4}$$

where $\mathbf{m}_i$ and $\mathbf{C}_i$ are the mean vector and covariance matrix of the data in class ω_i.

If the highest probability of a pixel falls below a specified value[1] a threshold can be set and the pixel won't be classified in any of the available classes. This circumstance will guarantee a certain degree of accuracy and is illustrated in Figure 2.2.

[1] For more information and the mathematical derivation see John A. Richards, *Remote Sensing Digital Image Analysis*, 5th *ed.*, Springer Science and Business Media, 2012, p. 250 ff.

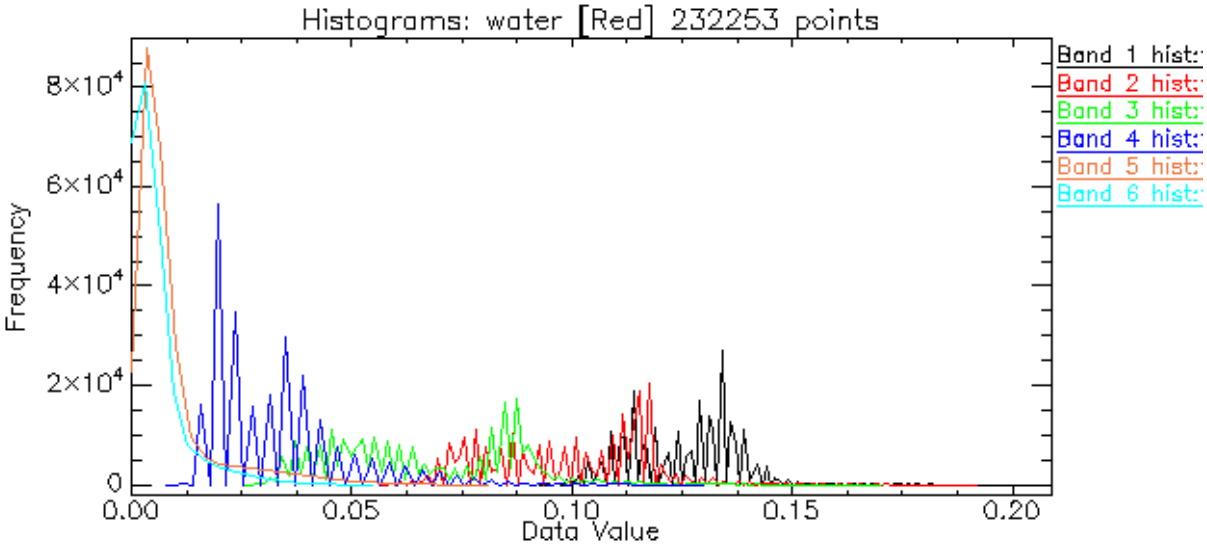

Figure 2.1: *Example of a histogram: water class in all six available bands*[1]

2.1.2 Minimum Distance Classification

The accuracy of the maximum likelihood classification (2.1.1) method depends on the number of training pixels used for each class. If this sufficient number is not possible, inaccurate valuation of the covariance matrix will lead to poor classifications. The minimum distance classification method depends only on the mean vector for each spectral class and does not make use of the covariance information. The training data is used to calculate class means and each pixel is then classified in the class of the nearest mean.

$$\mathbf{x} \in \omega_i \quad \text{if} \quad d(\mathbf{x}, \mathbf{m}_i)^2 < d(\mathbf{x}, \mathbf{m}_j)^2 \quad \text{for all} \quad j \neq i \tag{2.5}$$

in which $\mathbf{m}_i, i = 1...M$ are the means of the M classes, which are obtained from training data.

Similar to (2.3) the discriminant function of the minimum distance classifier is

$$\mathbf{x} \in \omega_i \quad \text{if} \quad g_i(\mathbf{x}) > g_j(\mathbf{x}) \quad \text{for all} \quad j \neq i$$

with

$$g_i(\mathbf{x}) = 2\mathbf{m}_i \cdot \mathbf{x} - \mathbf{m}_i \cdot \mathbf{m}_i \tag{2.6}$$

Table 2.1 shows an example for the class means in the image recorded in winter. Additionally the range in which the pixels are assigned to the classes is shown. The classification is employed on basis of the NDWI image, therefore the pixels have values between -1 (vegetation) and +1 (water).

[1] Band 6 is actually Landsat Band 7

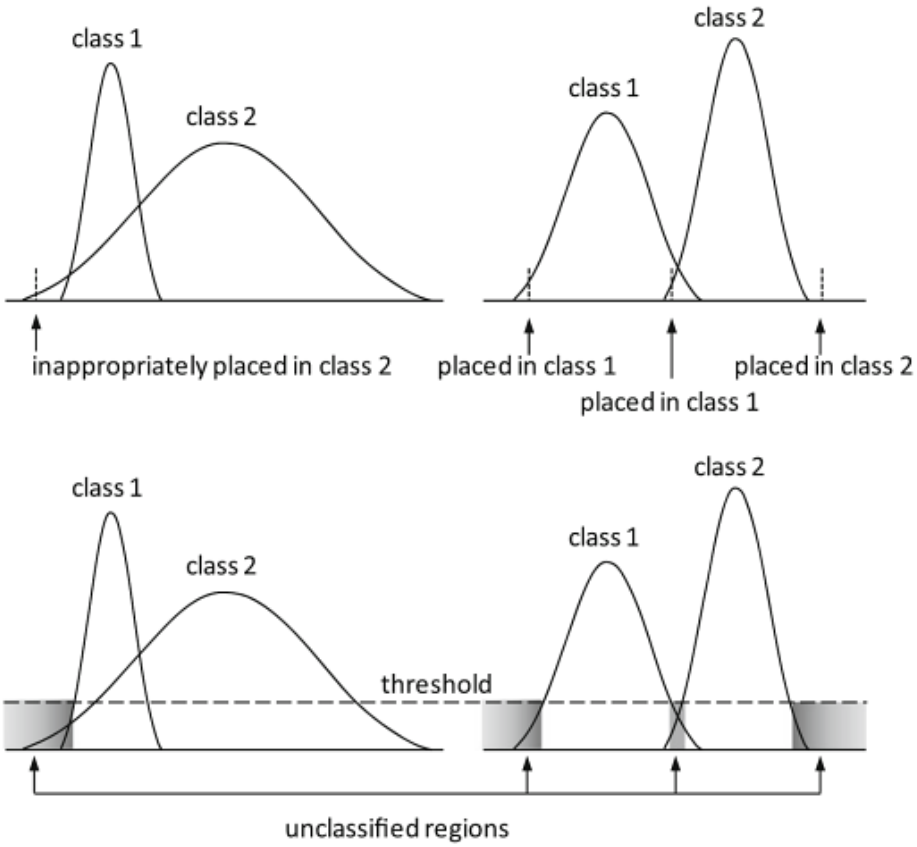

Figure 2.2: *Illustration of the use of thresholds to avoid questionable classification decisions [8]*

Table 2.1: *Class means, ranges and standard deviation in the classification of the fourth image*

Class	Minimum	Maximum	Mean	STD
Vegetation	-0.5861	-0.2078	-0.2722	0.0607
Dry soil	-0.2074	-0.0894	-0.1283	0.0301
Urban	-0.0894	-0.0425	-0.0668	0.0125
Wet soil	-0.0424	0.2221	-0.0003	0.0539
Water	0.2224	0.7287	0.4393	0.0974

Analogical to the thresholds in the maximum likelihood classifier, such can also be applied to the minimum distance classifier. They are usually specified in terms of a number of standard deviations from the class means. This classification technique is advantageous when the number of training pixels is limited or if linear separation of the classes is suspected [8].

2.1.3 Parallelepiped Classification

The parallelepiped classifier uses a simple decision rule, that is to find the upper and lower brightness values in each spectral dimension. Making use of the histograms of the individual spectral components in the available training data would be the most obvious solution to find these boundaries, as shown in Figure 2.3. For each class a multidimensional box or *parallelepiped* is formed (Figure 2.4). If a unknown pixel lies in between this box, it is assigned to that class.

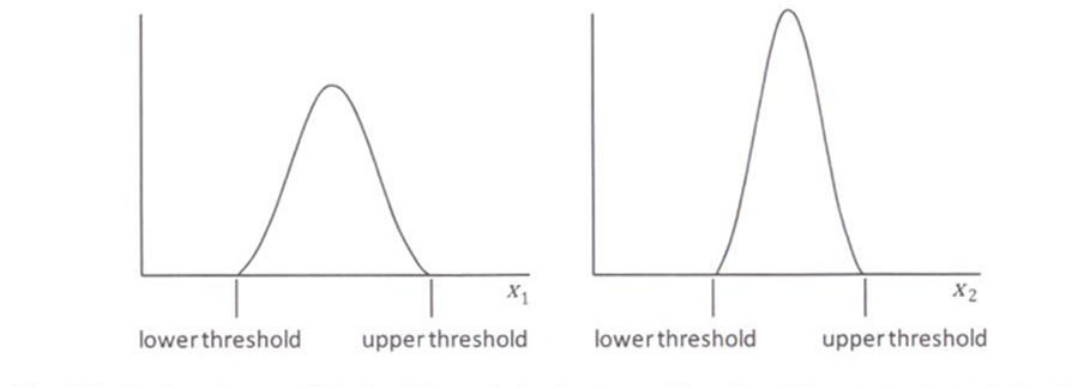

Figure 2.3: *Setting the parallelepiped boundaries by inspecting class histograms in each band*

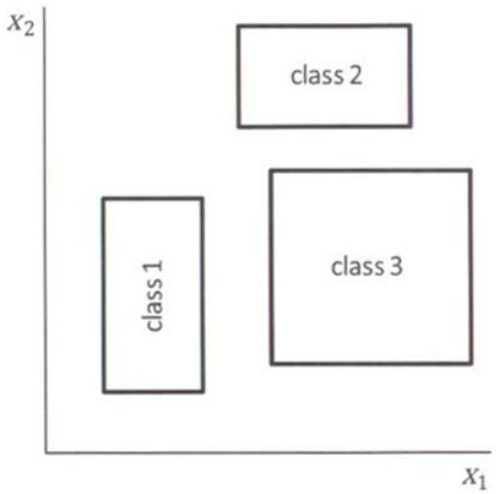

Figure 2.4: *A set of two dimensional parallelepipeds*

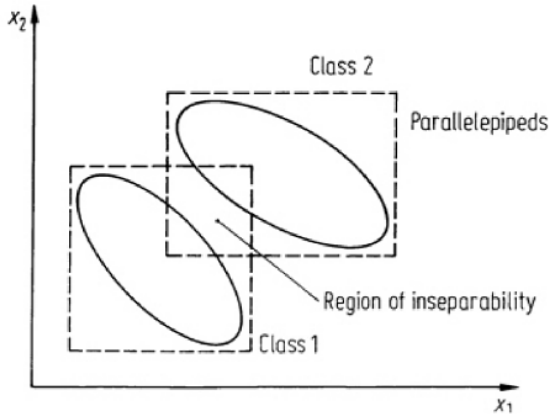

Figure 2.5: *Classification of correlated data showing regions of inseparability*

For correlated data some parallelepipeds can overlap, as illustrated in Figure 2.5. The classification software ENVI assigns pixels within this inseparable region to the last class matched. Another disadvantage of this classifier are gaps between the parallelepipeds. These areas will be designated as unclassified. Alike with the minimum distance classifier, there is no provision for prior probability of class membership with the parallelepiped rule, leaving the simple and fast computing algorithm as the only advantage in the parallelepiped classification method [2], [8].

2.1.4 Mahalanobis Distance Classification

The initial point of the mahalanobis distance classification is the discriminant function of the maximum likelihood classifier (2.4). If the sign is reversed, the function can be considered as a distance squared measure because the quadric entry has those dimensions and the other term is a constant [8]. We can define

$$d(\mathbf{x}, \mathbf{m}_i)^2 = \ln |\mathbf{C}_i| + (\mathbf{x} - \mathbf{m}_i)^T \mathbf{C}_i^{-1} (\mathbf{x} - \mathbf{m}_i) \tag{2.7}$$

and look for the smallest $d(\mathbf{x}, \mathbf{m}_i)$ to classify unknown pixels, similar to the minimum distance algorithm. Considered now that all class covariances are equal and given by $\mathbf{C}_i = \mathbf{C}$, which could be for example a class average, (2.7) can be reduced to

$$d(\mathbf{x}, \mathbf{m}_i)^2 = (\mathbf{x} - \mathbf{m}_i)^T \mathbf{C}_i^{-1} (\mathbf{x} - \mathbf{m}_i) \tag{2.8}$$

This squared distance is called the *mahalanobis distance*. The additional simplification $\mathbf{C} = \sigma^2 \mathbf{I}$ would result in the minimum Euclidean distance classifier of Section 2.1.2. Compared to the maximum likelihood classification method, this technique is faster and yet retains a degree of direction sensitivity via the covariance matrix $\mathbf{C}$ [8].

2.2 Unsupervised classification

Unsupervised classification is a method by which each pixel is assigned to a class without any prior knowledge of the existence or names of those classes. This process of grouping is called *clustering*. The user identifies the number of clusters to generate and which bands to use but takes no part in an algorithm's learning process directly. The produced cluster map now has to be compared to available reference data to identify the particular classes or clusters.
This method of classification is often useful for determinations prior to detailed analysis by the supervised methods from Section 2.1 [8].

2.2.1 Clustering Criteria

The task is to find groups of pixels that are somehow similar to each other. This similarity is measured in the spectral attributes recorded by the sensor used to acquire the data. The most common form of measurement in clustering procedures is usually a simple distance measure. Two examples would be the Euclidean distance (2.9) and the *city block* or *Manhattan* (2.10) distance. The Euclidean distance of two measurement vectors $\mathbf{x}_1$ and $\mathbf{x}_2$ whose similarity is to be checked is calculated as

$$\begin{aligned} d(\mathbf{x}_1, \mathbf{x}_2) &\mathrel{\widehat{=}} \|\mathbf{x}_1 - \mathbf{x}_2\| \\ &= \{(\mathbf{x}_1 - \mathbf{x}_2) \cdot (\mathbf{x}_1 - \mathbf{x}_2)\}^{1/2} \\ &= \left\{(\mathbf{x}_1 - \mathbf{x}_2)^T (\mathbf{x}_1 - \mathbf{x}_2)\right\}^{1/2} \\ &= \left\{\sum_{n=1}^{N} (x_{1n} - x_{2n})^2\right\}^{1/2} \end{aligned} \tag{2.9}$$

with $N \mathrel{\widehat{=}}$ number of spectral components. The *city block* (L_1) distance is given by

$$d_{L_1}(\mathbf{x}_1, \mathbf{x}_2) = \sum_{n=1}^{N} |x_{1n} - x_{x2n}| \tag{2.10}$$

The *city block* is way faster to compute at the cost of quality in spectral similarity within a given distance [8].

2.2.2 K-Means Clustering

The *k-means* clustering method is one of the most common approaches used in image analysis applications. It aims to partition all available measurement vectors into a preassigned number of clusters. After assigning an initial set of cluster centres the algorithm alternates between two steps:

- Reassign each pixel vector to the cluster with the closest mean using an appropriate distance metric between the pixel and cluster means. Euclidean distance is commonly used.
- Calculate new cluster means from each group.

These steps repeat until there is no significant change in the value of each pixel vector [8].

2.2.3 Isodata Clustering

The *Isodata* clustering uses the same algorithms as the *k-means* but with certain refinements such as splitting, merging and deleting clusters.

- **Merging clusters:** Sometimes two or more clusters are so close together that they represent unnecessary information content, in which they should be merged.
- **Deleting clusters:** Sometimes statistical distributions of certain pixels are important and must be available to generate reliable mean and covariance estimates, as for example in the maximum likelihood classification (see Section 2.1.1).
- **Splitting clusters:** Clusters with improper shapes in the spectral space can be split in two by pre-specifying a standard deviation in each spectral band beyond which a cluster should be halved [8].

Chapter 3

Results

For each of the four images, one for each season of the year, a spatial subset to show the training areas and the results of the six classifiers was defined. Along with that more information about the arrangement of the training areas and the statistic results for each classification will be presented in different tables and figures.

3.1 First Image: Spring

3.1.1 Training Data

As an example for training areas, Figure 3.1 shows a segment of the first Image to be classified created with the software ENVI. Five land cover classes (Regions of interest; ROI) were defined: Water (blue), vegetation (green), dry soil (yellow), wet soil (orange) and urban area (cyan).

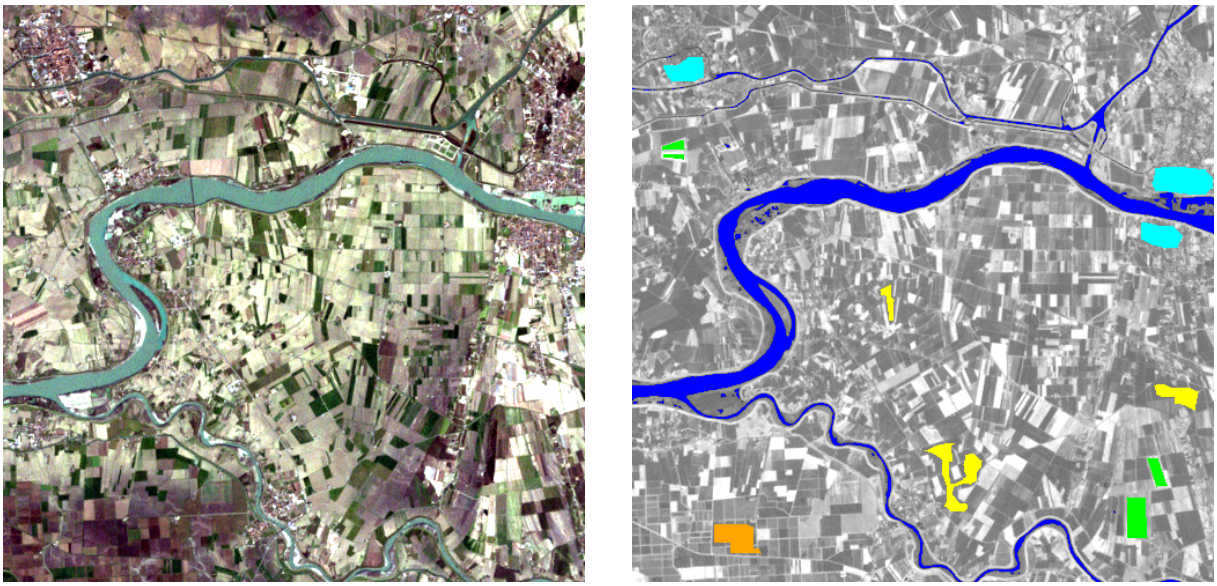

(a) *True colour (321)* ***(b)*** *NDVI image with training areas*

Figure 3.1: *Image segment to be classified; consisting of different land cover classes*

The amount of training pixels for each class and their related colour is shown in Table 3.1. The training pixels for the water class were created by using a band threshold with values from -1

Table 3.1: *Regions of interest with their corresponding amount of pixels and colours*

ROI Name	Colour	Pixels	Polygons[1]	Points
Water	Blue	232,253	0/0	232,253
Vegetation	Green	8,167	28/8,167	0
Dry soil	Yellow	20,467	24/11,104	9,363
Wet soil	Orange	29,169	26/12,266	16,903
Urban	Cyan	5,816	9/5,816	0

to -0.1 from a NDVI image as a region of interest. Every pixel in between these values is now used as a training pixel. The other training areas were generated with polygons, rectangles, ellipses or expanded single points in the RGB image.

3.1.2 Classified Images

Figure 3.2 shows a spatial subset of the full image as a negative colour image. This subset includes the five land cover classes as well as critical sectors in which the classification is ambiguous. The results of the six classifiers are depicted in Figure 3.3.

Figure 3.2: *Subset of the season 1 image as a negative colour image (432). The image shows vegetated area as well as bare soil. The urban area in the center was the critical sector to be classified and shows different results in each of the classifiers.*

[1]Amount of polygons and how many training pixels they contain in total; remaining pixels are created from expanding single pixels or from band thresholds

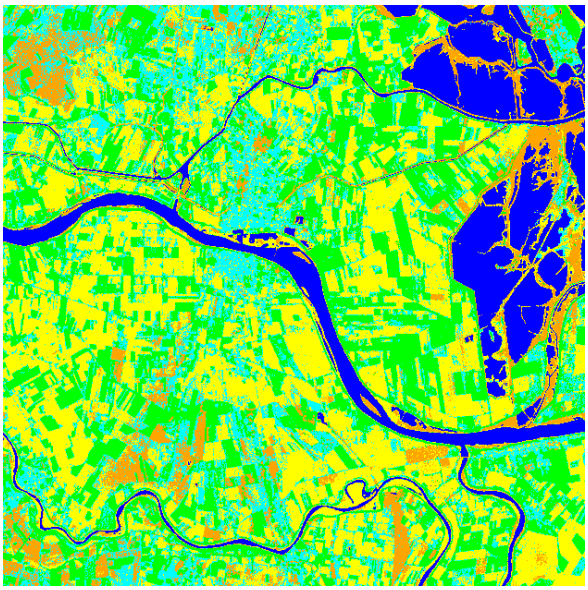

(a) *Maximum Likelihood Classifier*

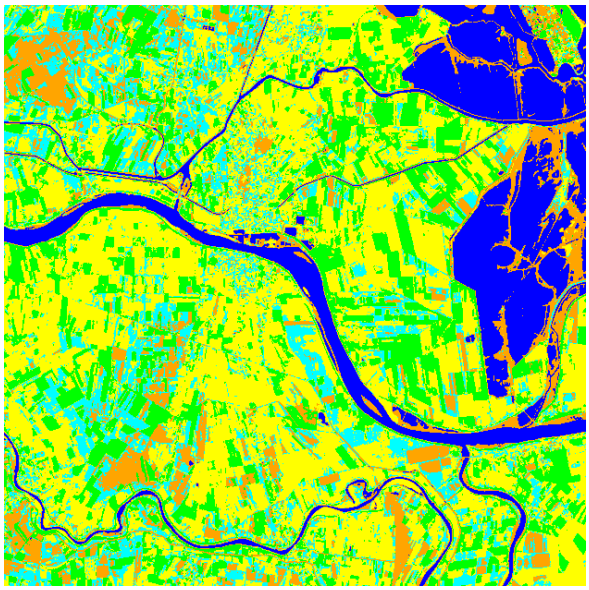

(b) *Minimum Distance Classifier*

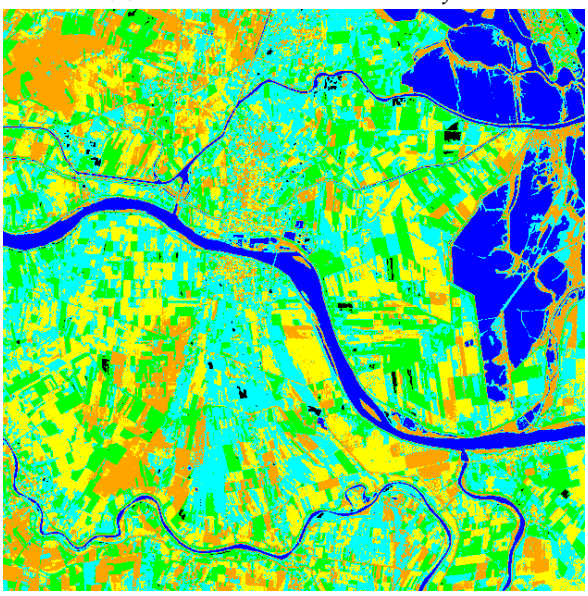

(c) *Parallelepiped Classifier*

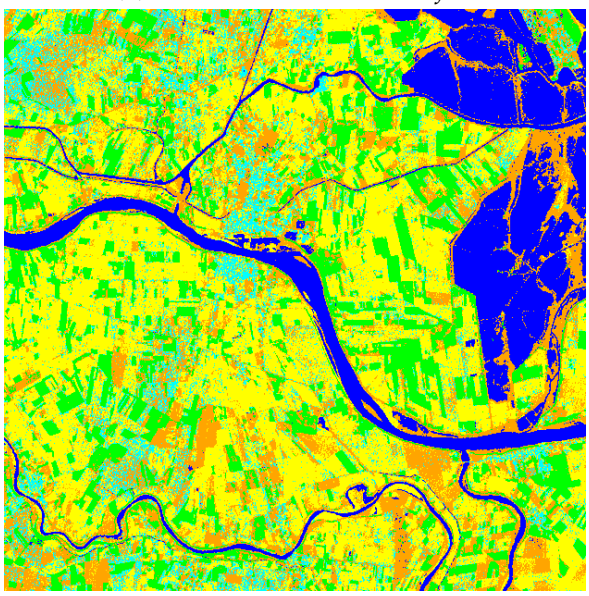

(d) *Mahalanobis Distance Classifier*

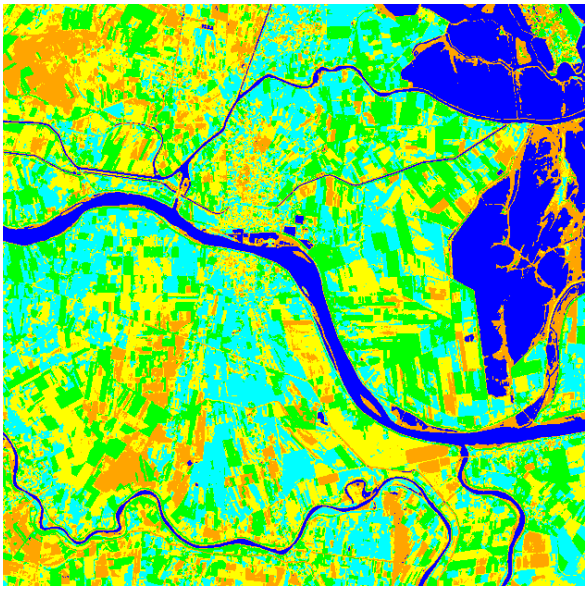

(e) *K-Means Clustering*

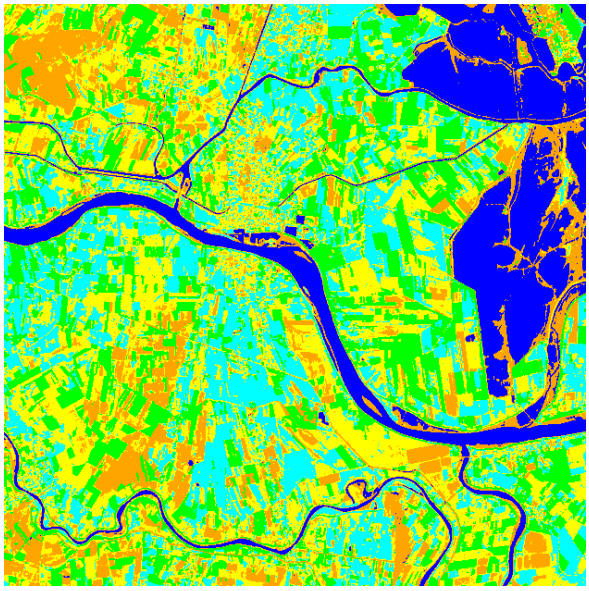

(f) *Isodata Clustering*

Figure 3.3: *First image: Spring classification results*

Most images were generated without any thresholds or limitations. Only in the minimum distance classifier (Figure 3.3b) a maximum standard deviation from the mean limitation of the factor 2 in the urban class has been applied. Otherwise too many pixels would have been classified to the this class. For proper distribution of the pixels in the parallelepiped classification (Figure 3.3c) a couple of thresholds have been used. A factor of 3 in the water class, 2 in vegetation, 1.3 in bare and 2.5 in wet soil and the urban class was stretched by the factor 7 from the mean value. This way only 0.27 % of the pixels were left as unclassified.

The properties in the K-means algorithm (Figure 3.3e) was limited to 10 iterations or less than 3 % of the pixels change their class. Also no maximum standard deviation or distance error from the mean in each class were applied. Same properties apply to the Isodata clustering (Figure 3.3f) but additionally the algorithm could chose from five up to seven classes. It still classified the image into five classes. On the first sight we see no difference in the unsupervised classified images but they can primarily be separated by the number of pixels in the wet soil and the urban area class.

3.1.3 Discussion

A precise notation of the percentage of pixels in each class for the single classified images is given in Table 3.2.

Table 3.2: *Spring image statistics results*

Classifier	Unclassified	Water	Vegetation	Dry soil	Wet soil	Urban
Maximum likelihood	0 %	6.12 %	23.22 %	33.51 %	13.84 %	23.32 %
Minimum distance	0 %	6.47 %	18.51 %	29.92 %	20.84 %	24.26 %
Parallelepiped	0.27 %	5.77 %	19.28 %	25.44 %	28.76 %	20.48 %
Mahalanobis distance	0 %	6.78 %	16.55 %	29.17 %	29.54 %	17.96 %
K-Means clustering	0 %	6.61 %	20.74 %	34.95 %	25.43 %	12.27 %
Isodata clustering	0 %	6.66 %	19.51 %	34.67 %	28.34 %	10.81 %

As we can see, the amount of water varies between 5.77 % and 6.78 % or in area units: between 207.9405 km^2 and 244.2861 km^2 which makes a difference of 36.3456 km^2. The maximum likelihood (Figure 3.3a) and the mahalanobis distance (Figure 3.3d) classifier outperform as far as the urban area is concerned while the unsupervised classifiers couldn't distinguish between soil and urban area but they still remained very accurate in the river boundaries and the oceanic region.

3.2 Second Image: Summer

3.2.1 Training Data

The second image takes place in early summer of the year 2001. The whole area suffers from high cloud coverage which can be seen in Figure 3.4a. It is almost impossible to get accurate classification results in the regions right beneath the clouds and in the cloud-shadowed areas.

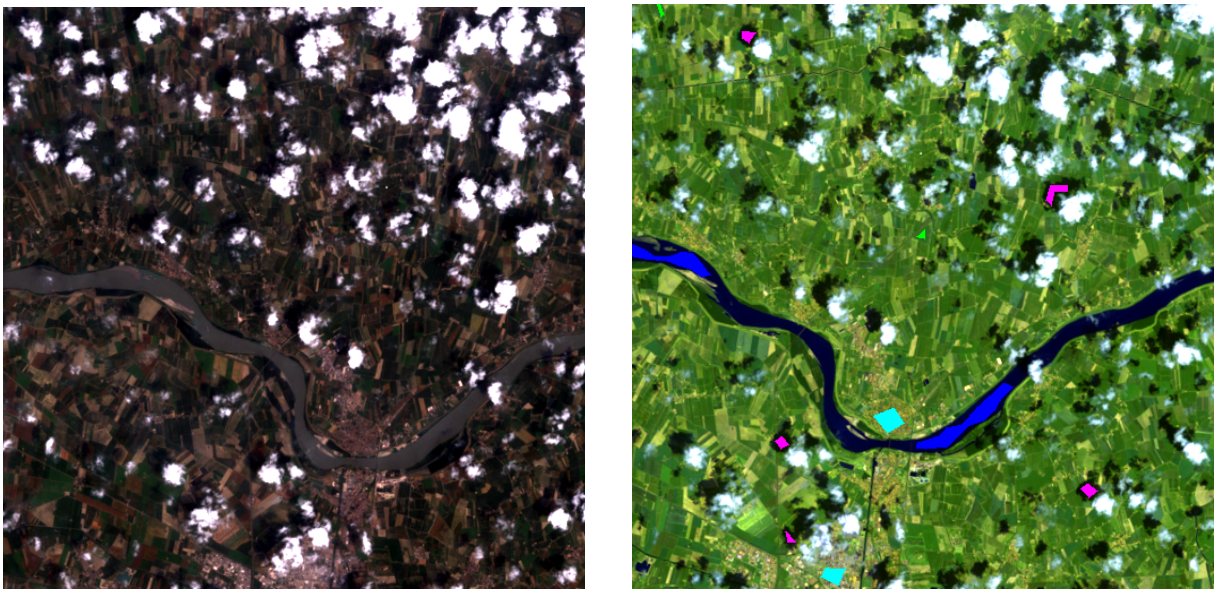

(a) *True colour (321)* ***(b)*** *Natural like image (752); training areas*

Figure 3.4: *Spatial subset of the image recorded in summer; The whole image suffers from high cloud coverage and shaded areas*

With help of the false colour image (432) and the NDVI two additional classes to examine these areas were defined. The other classes will be retained but a discrimination in different soil features was not necessary anymore, which gives us a total of seven land cover classes. Like in the season 1 image the training pixels for the water class were generated with help of the NDVI image but this time in form of polygons. The best examination of the vegetated areas could be provided with a 742 band combination and the same goes for soil features. The total amount of pixels for each region of interest is depicted in Table 3.3 and a small subset is pictured in Figure 3.4b.

Table 3.3: *Regions of interest with their corresponding amount of pixels and colours*

ROI Name	Colour	Pixels	Polygons[1]
Water	Blue	9,964	25/9,964
Vegetation	Green	9,111	33/9,111
Soil	Yellow	5,301	19/5,301
Urban	Cyan	2,888	12/2,888
Cloud	White	2,620	12/2,620
Shadow	Blue	1,107	12/1,107

3.2.2 Classified Images

The performance of the six classifiers and how they classified the cloud-covered areas are shown in Figure 3.5 in the same manner as in the previous section. Again a small subset which includes all critical sectors of the whole image will represent the results for this image.

[1] Amount of polygons and how many training pixels they contain in total; remaining pixels are created from expanding single pixels or from band thresholds

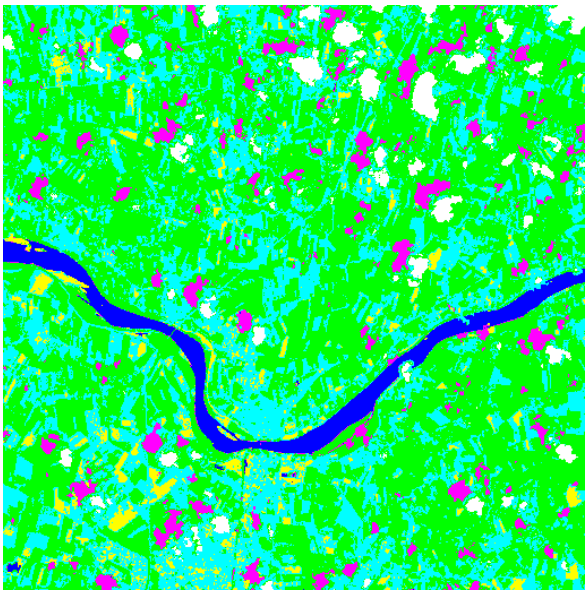

(a) *Maximum Likelihood Classifier*

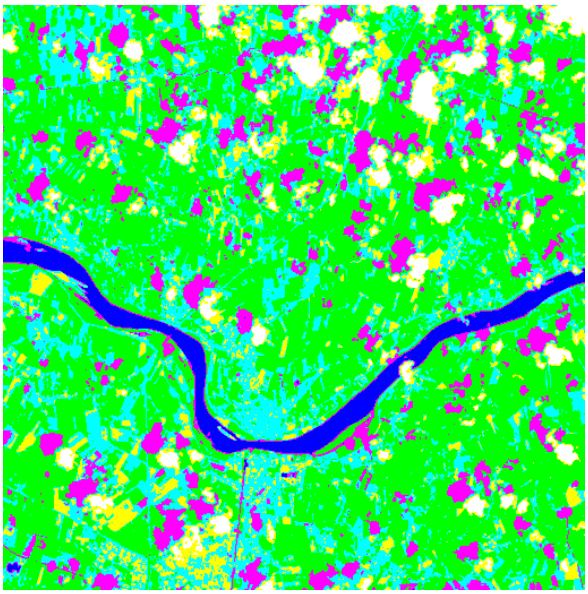

(b) *Minimum Distance Classifier*

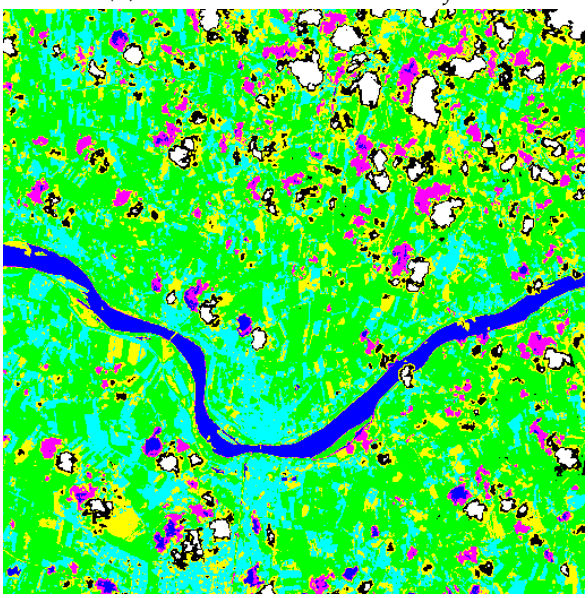

(c) *Parallelepiped Classifier*

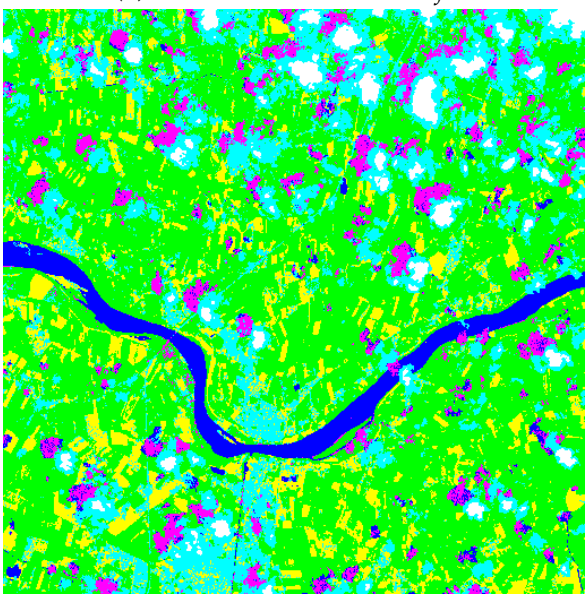

(d) *Mahalanobis Distance Classifier*

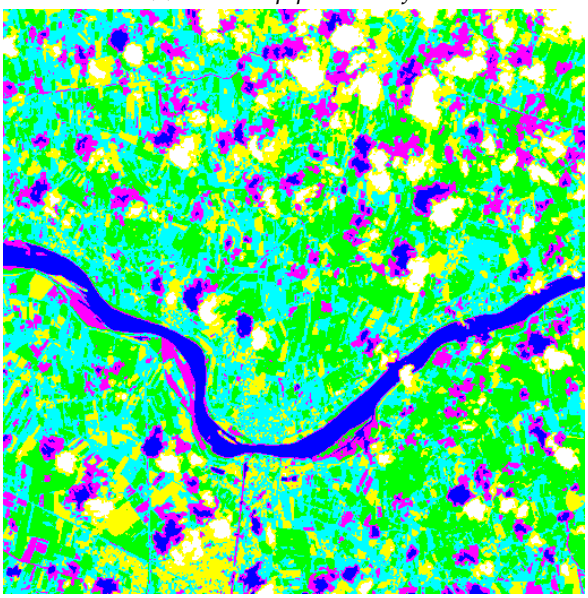

(e) *K-Means Clustering*

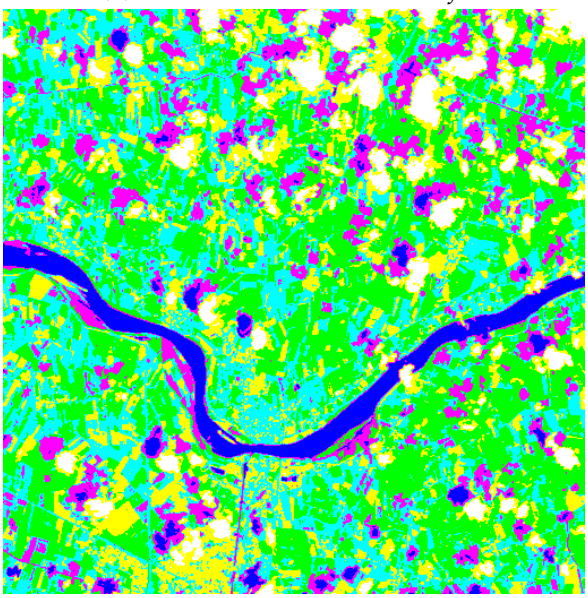

(f) *Isodata Clustering*

Figure 3.5: *Second image: Summer classification results*

Again as little thresholds as possible were applied to classify as much pixels as possible. Some distribution corrections set in the parallelepiped (Figure 3.5c) and the mahalanobis distance classification (Figure 3.5d). Wihtout thresholds in the first case, almost the whole image would have been classified to the vegetation class and in the mahalanobis distance classification huge errors in the water and shadow classes made a usage of thresholds inevitable.

The properties for the K-means classification (Figure 3.5e) were the same as in the image recorded in spring, but this time with a limitation to six classes. In the Isodata clustering (Figure 3.5f) a minimum of six and a maximum of eight classes were chosen, otherwise the algorithm would have set the number of classes down to five and merged the water and shadow class together. This way the number of classes equals the same in all pictures.

3.2.3 Discussion

Table 3.4 shows the distribution of pixels in the single classes similar to Table 3.2 from spring. If we consider that cloud-covered and shadows area is lost data and add these two classes to the unclassified pixels we will get a certain percentage of lost data for each of the classifiers.

Table 3.4: *Summer image statistics results*

Classifier	Unclass.	Water	Vegetation	Soil	Urban	Cloud	Shadow
Max. likelihood	0 %	5.61 %	45.04 %	6.46 %	35.09 %	3.41 %	4.40 %
Minimum distance	0 %	5.71 %	34.93 %	7.80 %	35.01 %	4.18 %	12.37 %
Parallelepiped	5.21 %	6.54 %	41.16 %	14.77 %	25.36 %	3.25 %	3.70 %
Mahalanobis dist.	0 %	8.18 %	41.23 %	15.25 %	28.31 %	2.86 %	4.17 %
K-Means clustering	0 %	8.64 %	16.67 %	16.00 %	36.14 %	5.46 %	17.11 %
Isodata clustering	0 %	7.51 %	19.85 %	16.65 %	36.36 %	5.46 %	14.18 %

This way the mahalanobis classifier (Figure 3.5d) would show the best classification as far as the data loss in the whole scenery is concerned. The most classified pixels, especially in the cloud class, look very accurate, however this classifier has difficulties in separating the shadowed areas from the water areas. Also a misclassification in the oceanic region appeared.

The maximum likelihood (Figure 3.5a) along with the minimum distance classifier (Figure 3.5b) performed pretty well in the shadowed and cloud-covered areas and did not classify any significant areas in a wrong way. Only cropped fields with high moisture content were classified differently into the vegetation or accordingly in the shadow class. The parallelepiped classifier (Figure 3.5c) assigned these pixels into the water class and since this class is the one of highest interest, a misclassification is very disadvantageous. Additionally this classifier misinterpreted some cloud shadows as an area of water content. This circumstance of misclassification in this image is shown in Figure 3.6.

In the classification images provided by the unsupervised methods similar effects appeared. The K-means classifier (Figure3.5e) shows the same errors as the parallelepiped classifier but in an even bigger impact which explains the 8.64 % water content in the whole scenery. The Isodata classifier (Figure 3.5f) eliminated these errors in the shadowed areas but remains them in areas of high water content. Still this classification can be referred as the most accurate in this season.

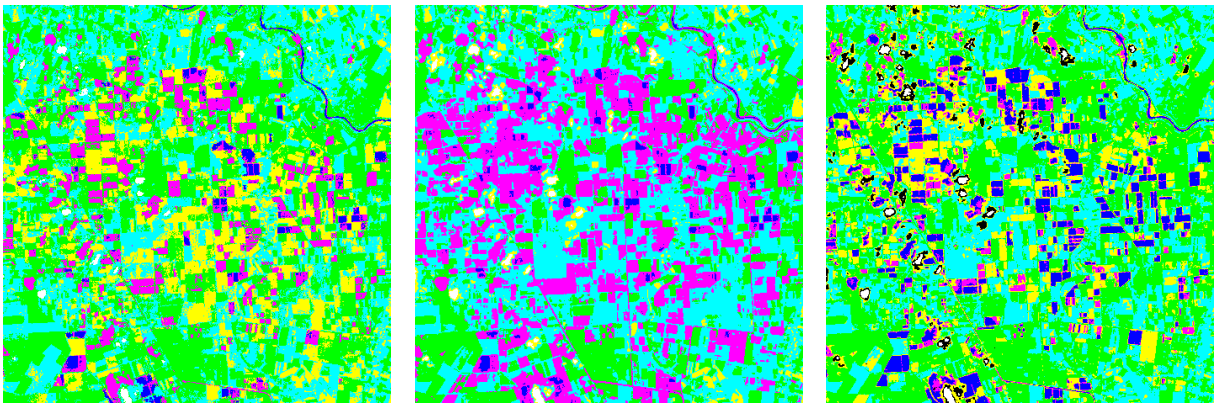

(a) Maximum likelihood *(b)* Minimum distance *(c)* Parallelepiped

Figure 3.6: *Misclassified area of the summer image*

3.3 Third Image: Autumn

3.3.1 Training data

The image of the third season takes place in late summer and shows some brightness issues in the southern part of the image as seen in Figure 3.7a. The same land cover classes as in season 1 were defined: Water, vegetation dry and wet soil and an urban class.

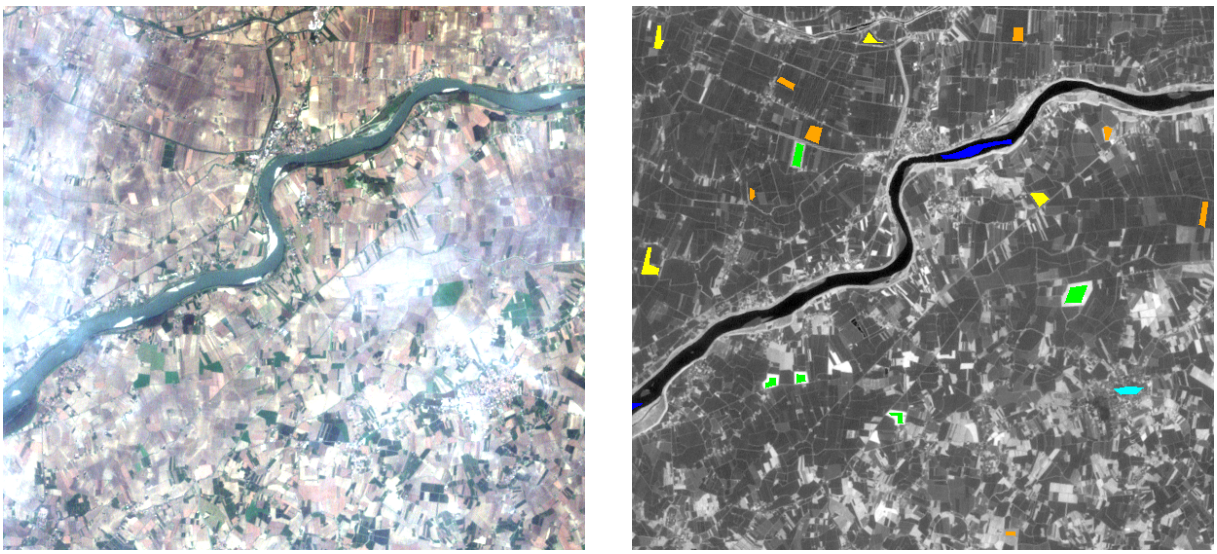

(a) True colour (321); brightness issues *(b)* NDVI image with training areas

Figure 3.7: *Spatial subset of the autumn image; An area in the south suffers from brightness issues*

As seen in Figure 3.7b the brightness issues are completely diminished in the NDVI image. Therefore this index would operate perfectly as a base for our training data. The colours and the approach to the training areas remained the same as in the previous sections.

3.3.2 Classified Images

The classification results for the third image are presented in Figure 3.8.

No thresholds were applied to the maximum likelihood classification (Figure 3.8a) and only small limits in the wet soil and urban class were set in the minimum distance image (Figure 3.8b). Same goes for the mahalanobis distance classifier (Figure 3.8d). The water class in the parallelepiped classification (Figure 3.8c) was highlighted while the vegetation and dry soil class has been narrowed down.

Adding additional classes in the unsupervised classifications was of no avail. The algorithm just classified soils and rocks into more and more classes of different moisture content. Thus the properties in the K-means (Figure 3.8e) and the Isodata classifier (Figure 3.8f) remained the same as in the first season.

3.3.3 Discussion

To illustrate how the classifiers performed in an image affected by brightness issues Table 3.5 gives us a short overview of the assignment of pixels in each class in the same way as in the previous sections.

Table 3.5: *Autumn image statistics results*

Classifier	Unclassified	Water	Vegetation	Dry soil	Wet soil	Urban
Maximum likelihood	0 %	5.21 %	13.02 %	21.87 %	22.24 %	37.66 %
Minimum distance	0 %	7.86 %	13.20 %	23.87 %	19.09 %	35.98 %
Parallelepiped	2.06 %	6.38 %	14.66 %	24.47 %	29.04 %	23.40 %
Mahalanobis distance	0 %	10.96 %	14.14 %	29.35 %	11.20 %	34.34 %
K-Means clustering	0 %	6.27 %	15.38 %	20.08 %	24.37 %	33.93 %
Isodata clustering	0 %	6.31 %	14.08 %	19.18 %	26.23 %	34.20 %

If we take a closer look at Figure 3.8 the supervised classifiers assigned most of the brightened area to the urban class. An exception is the minimum distance classifier. The unsupervised classifiers led to better results in this case.

The maximum likelihood and the mahalanobis distance classifier were not able to generate firm water boundaries and show a significant amount of misclassified pixels in the oceanic region and in the separation between wet soil and water (see Figure 3.9. These errors could not be corrected by applying thresholds or excluding single spectral bands from the classification.

Even though the minimum distance and the parallelepiped classifier had some issues in the detection of thin water layers their water boundaries around the river seem to be pretty accurate and low in misclassified pixels. The images created by

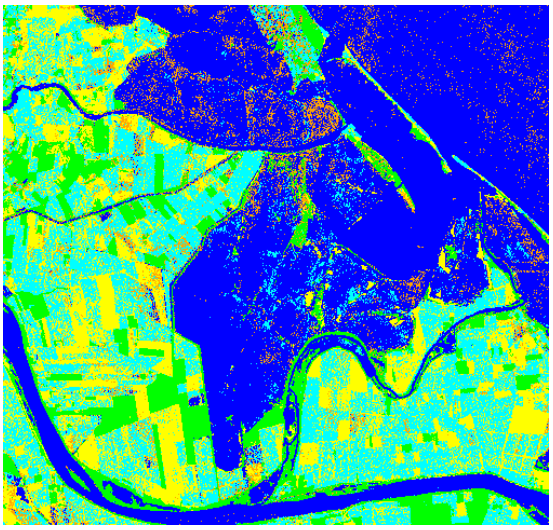

Figure 3.9: *Errors in the mahalanobis distance classification*

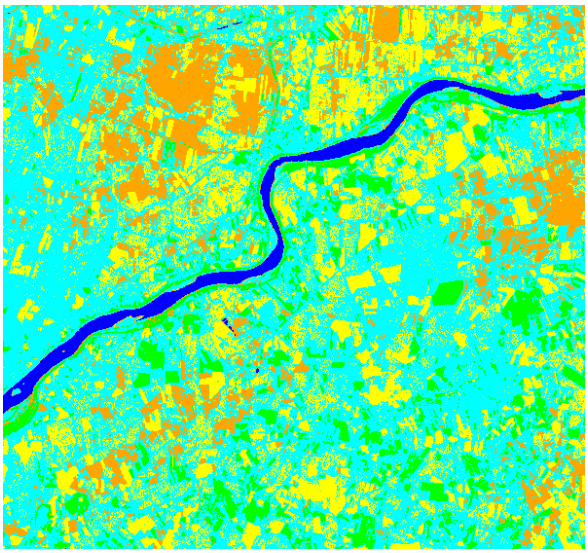

(a) *Maximum Likelihood Classifier*

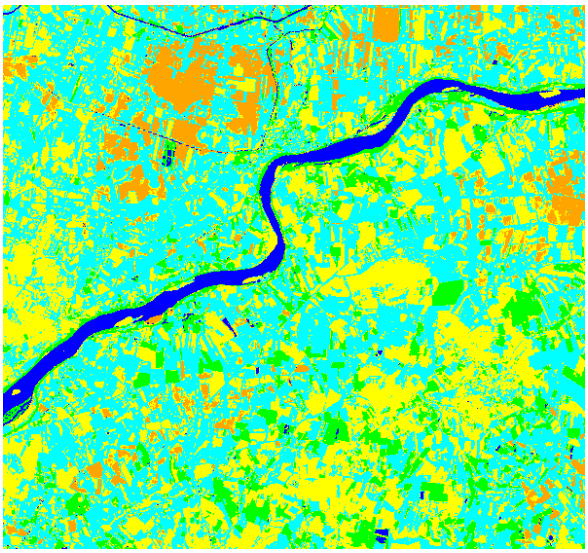

(b) *Minimum Distance Classifier*

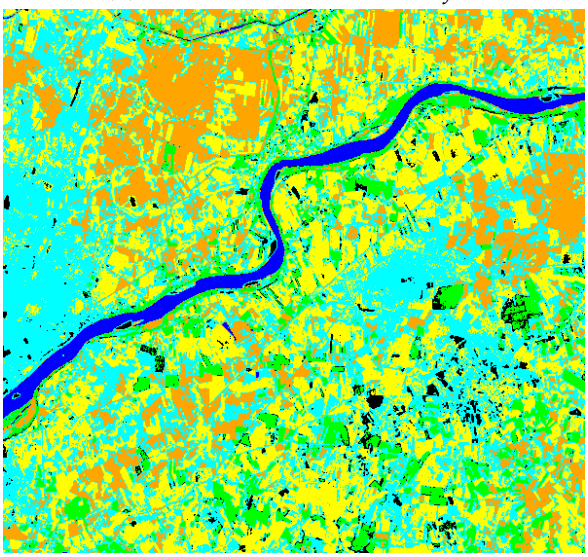

(c) *Parallelepiped Classifier*

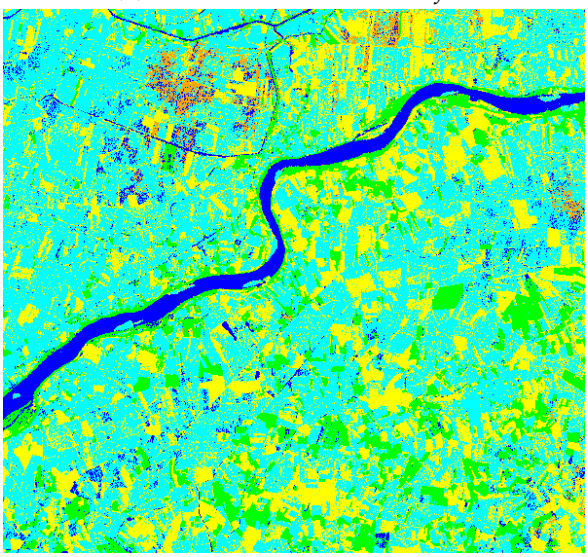

(d) *Mahalanobis Distance Classifier*

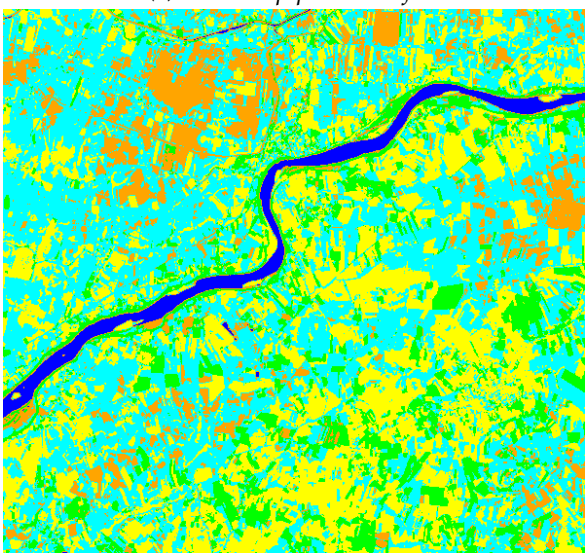

(e) *K-Means Clustering*

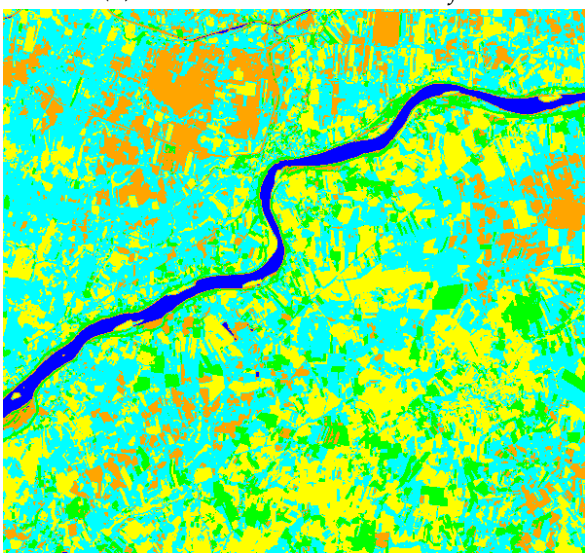

(f) *Isodata Clustering*

Figure 3.8: *Third image: Autumn classification results*

the unsupervised methods show a high similarity to the minimum distance image. Only a little area affected by the brightness issues was classified in a wrong way in the unsupervised classification methods.

3.4 Fourth Image: Winter

3.4.1 Training Data

The fourth and last image was recorded at the end of the year 2001. As seen in Figure 3.10a the true colour RGB implementation won't be of any practical use. The brightness values in the swath wary widely through the whole spectrum by what the image almost appears as a black and white image. The NDVI image does not help us either but the *Normalized Difference Water Index* (Figure 3.10b) in collaboration with some false colour images will lead to reasonable training areas (Figure 3.11). Also the histogram of the NDWI image has been balanced to a minor extent.

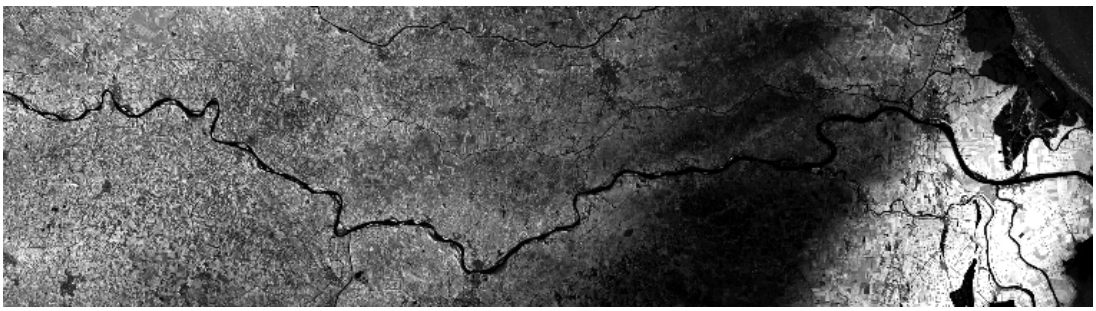

(a) *True colour image (321) of the whole swath*

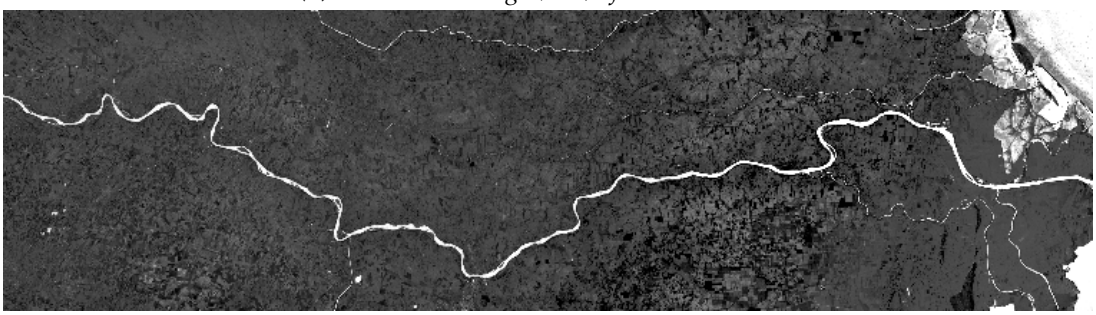

(b) *Normalized Difference Water Index (NDWI)*

Figure 3.10: *True colour (321) and NDWI image of the whole swath*

3.4.2 Classified Images

The maximum likelihood classification image in Figure 3.12a was computed based on the whole spectral subset, which means that all possible spectral bands were used (band 1 to 5 and band 7). Also no thresholds were applied. In the parallelepiped (Figure 3.12c) and the mahalanobis distance classifier (Figure 3.12d) only band 5 and 7 were used to guarantee as much

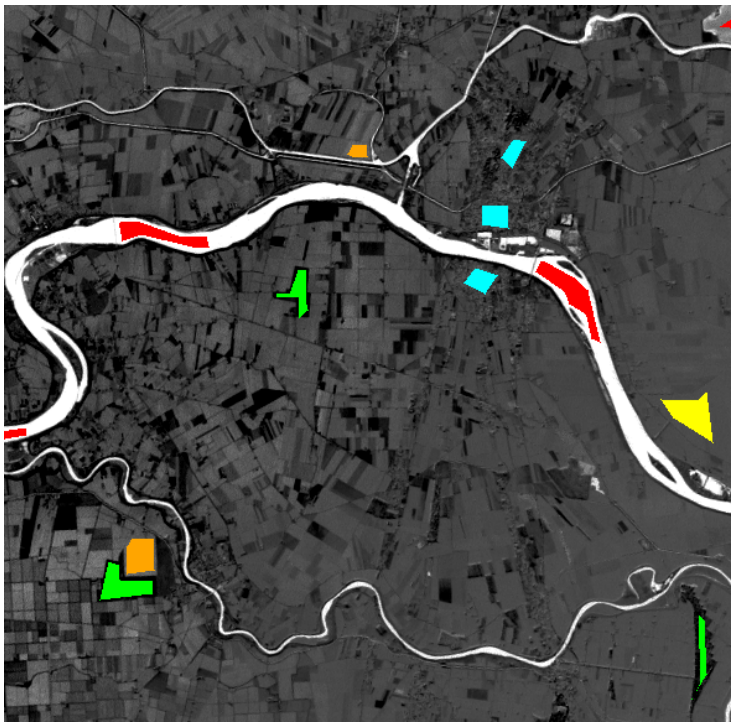

Figure 3.11: *NDWI subset with training areas*

atmospheric penetration as possible. Otherwise those classifiers would have totally misclassified the dimmed and the brightened area in the bottom right of the image. Limitations to all classes in the parallelepiped classification were applied but apart from that the water class was stretched. This way a various amount was pixels were left as unclassified but at least the water area in the dimmed area shows reliable results.

The minimum distance classifier (Figure 3.12b) along with the unsupervised methods (Figures 3.12e and 3.12f) were classified based on the NDWI image. Irrespective of the settings the usual image did not lead to any accurate results.

3.4.3 Discussion

Table 3.6 will show us if there will be any significant difference in classification images computed from the NDWI or the usual image on different spectral subsets.

Table 3.6: *Winter image statistics results*

Classifier	Unclassified	Water	Vegetation	Dry soil	Wet soil	Urban
Maximum likelihood	0 %	5.42 %	9.87 %	51.70 %	18.96 %	14.04 %
Minimum distance	0 %	4.71 %	4.80 %	35.07 %	13.90 %	41.52 %
Parallelepiped	5.86 %	5.74 %	14.32 %	27.41 %	35.56 %	11.12 %
Mahalanobis distance	0 %	7.58 %	9.10 %	47.07 %	17.68 %	18.57 %
K-Means clustering	0 %	4.67 %	6.42 %	27.34 %	8.03 %	53.54 %
Isodata clustering	0 %	4.60 %	4.71 %	24.38 %	6.56 %	59.71 %

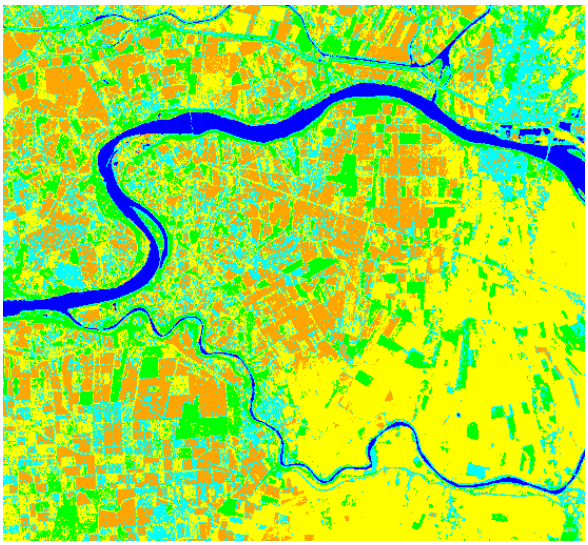

(a) *Maximum Likelihood Classifier*

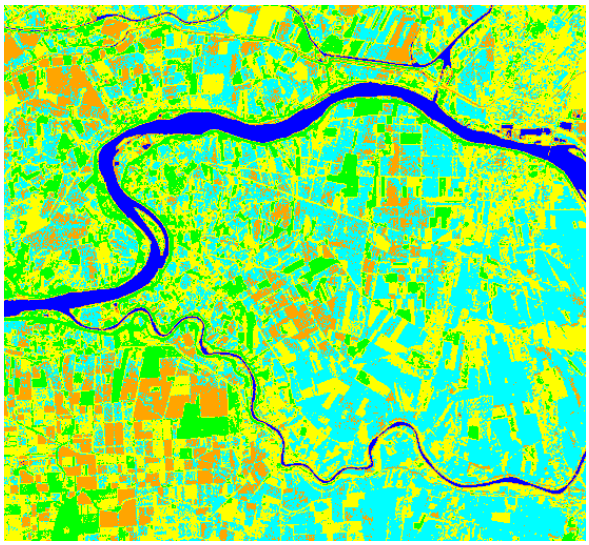

(b) *Minimum Distance Classifier*

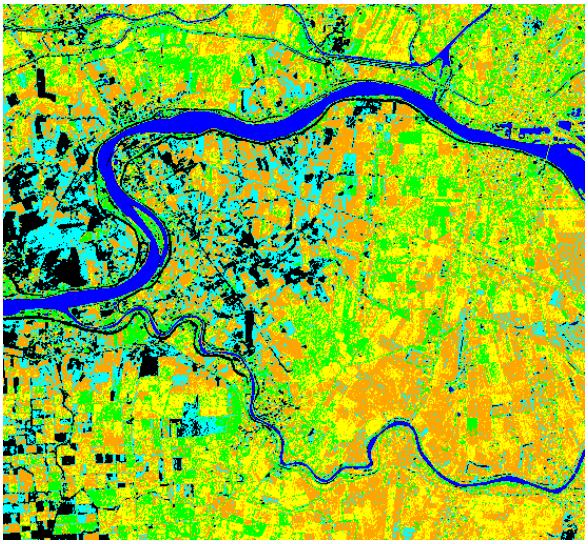

(c) *Parallelepiped Classifier*

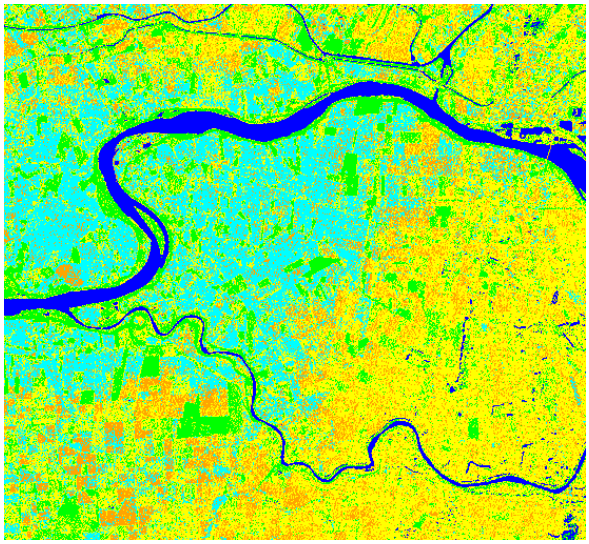

(d) *Mahalanobis Distance Classifier*

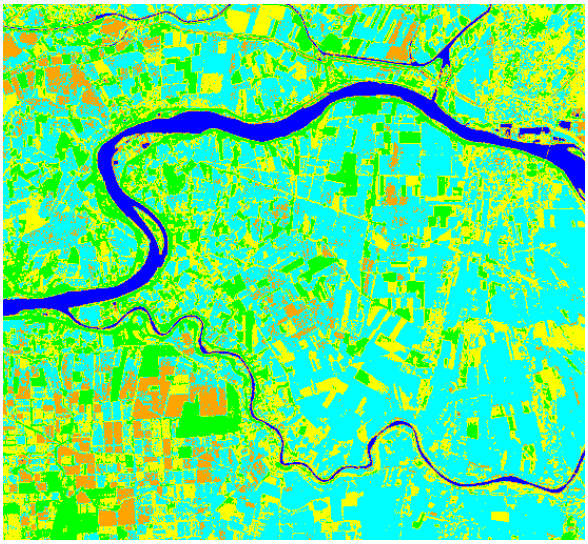

(e) *K-Means Clustering*

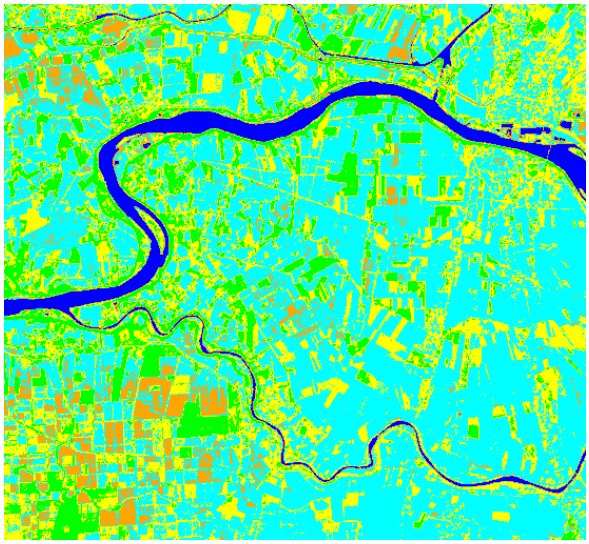

(f) *Isodata Clustering*

Figure 3.12: *Fourth image: Winter classification results*

The maximum likelihood classifier (Figure 3.12a) showed a great performance in the urban and vegetation classes but assigned the dimmed area almost completely into the wet soil class. The mahalanobis distance classifier (Figure 3.12d) on the other hand assigned these pixels to the urban class and overall looks very pixelated without any fixed structure. In the image created by the parallelepiped classifier (Figure 3.12c) many pixels were left as unclassified especially in the vegetated areas in the dimmed part of the image.

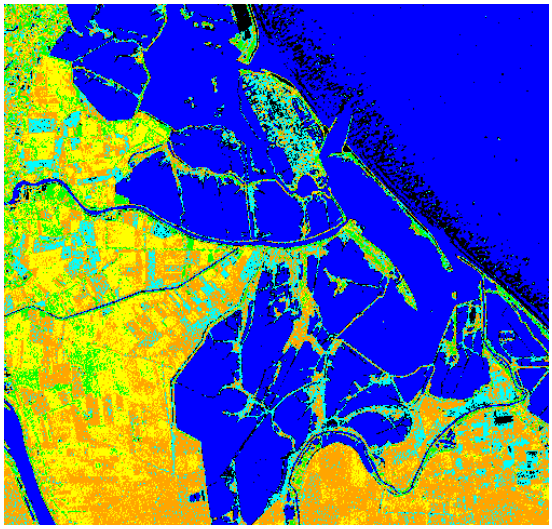

Figure 3.13: *Error in the coastal region; represented in the parallelepiped classification*

The minimum distance classification along with the unsupervised classifiers did not really classified an urban class. It is more a leftover class for farmland and urban features. It is evident that this similarity comes from the NDWI image as a basis for the classification.

An error in the coastal region appeared in almost every classified image. A subset from this area is represented in Figure 3.13. The parallelepiped classifier left the pixels around the coast as unclassified while the maximum likelihood and the mahalanobis distance classifiers assigned them to the urban and the vegetation class. Since this area should contain sand or turbid water, the water or the wet soil class would be the most obvious classification. The minimum distance and the unsupervised classifiers applied to this solution.

Chapter 4

Validation

To give precise differentials in the distance between the river widths calculated from the classifications and the results from in situ measurements two spots alongside the river were chosen as seen in Figure 4.1. At these two spots, located in Sermide and Pontelagoscuro, a direct comparison is performed.

(a) *Whole swath; locations of Sermide and Pontelagoscuro*

(b) *Sermide*

(c) *Pontelagoscuro*

Figure 4.1: *Areas for a comparison with an in-field surveillance*

In order to measure the exact river widths in the classified images the images are now converted to a binary water-mask. As an example the water-mask from the spring image Isodata classification is shown in Figure 4.2a. Since there is no significant difference in the single masks, the display of all masked image is not necessary. Combination of the mask and other images with simple mathematical operators can improve the visual results. In Figure 4.2b a simple

multiplication of the values from the NDVI image and the binary water mask has been applied.

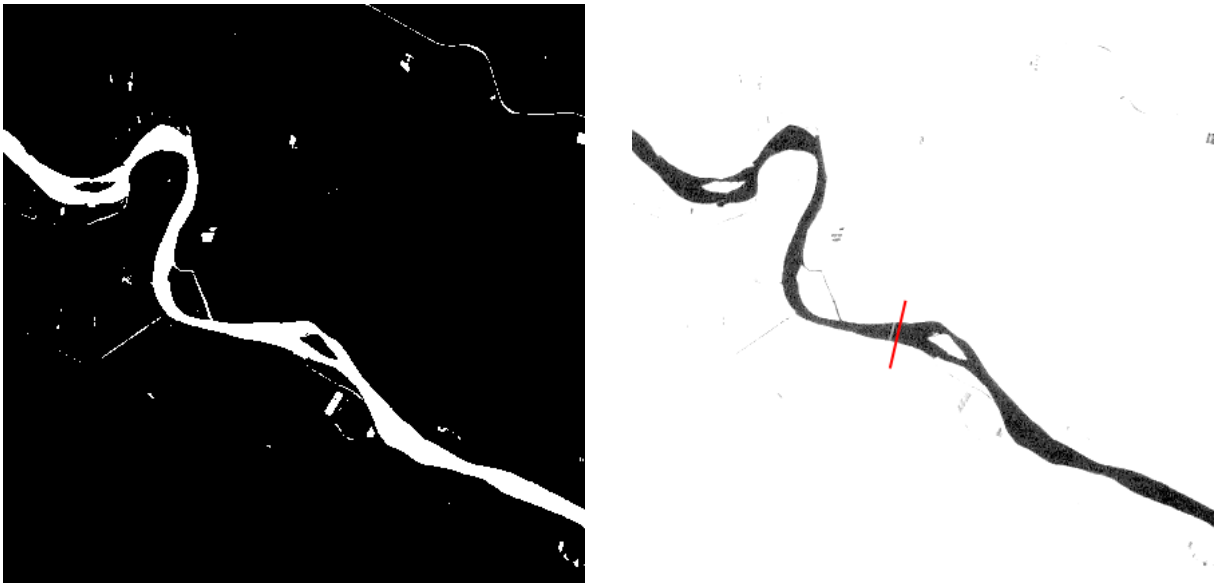

(a) *Isodata water mask*

(b) *Water mask multiplied with the NDVI image; River profile to be measured*

Figure 4.2: *Water mask example: Gauge spot Sermide*

With help of the measurement tool in ENVI precise measurements at desired locations (Red line in Figure 4.2b) can now be applied. The results from each classification can now be compared to an in-field surveillance to assess the performance of the different classifiers.

4.1 In Situ Results

Between 1995 and 2011 profile measurements alongside the river have been taken regularly. The location of these profiles are shown in Figure 4.3 and as mentioned earlier two of these profiles are chosen for closer investigation. They are depicted in Figure 4.4. The river widths at these two spots for all four seasons of the year 2001 are depicted in Table 4.1. They will serve as reference values for the following performance analysis. We can see that the river widths decline constantly throughout the year and if we look at past and future years from the date this measurements were taken this circle will repeat every year. The rivers profile in Sermide shows an abrupt slope together a levee (see Figure 4.4a), probably due to heavy flooding in this area, by what the river width does not differ very much throughout the year.

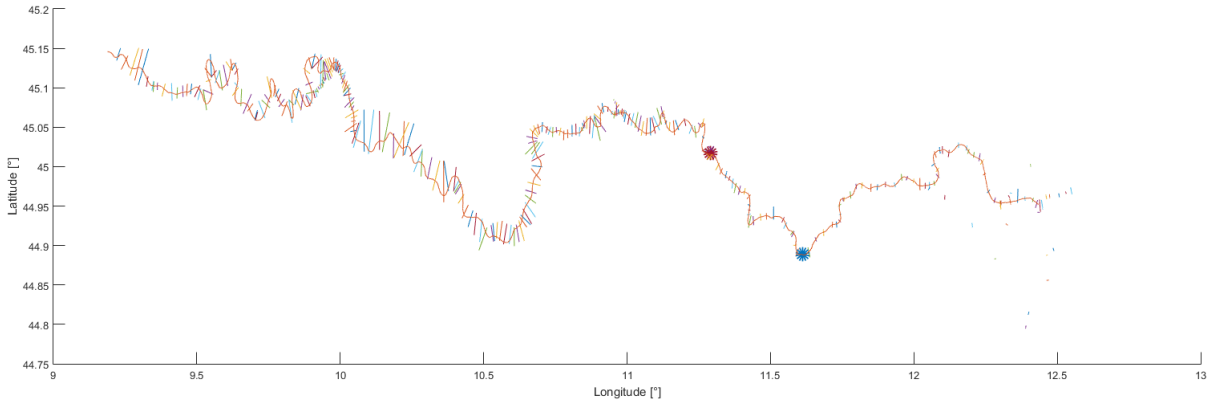

Figure 4.3: *Profile measurements alongside the Po river; Gauge spots Sermide and Pontelagoscuro*

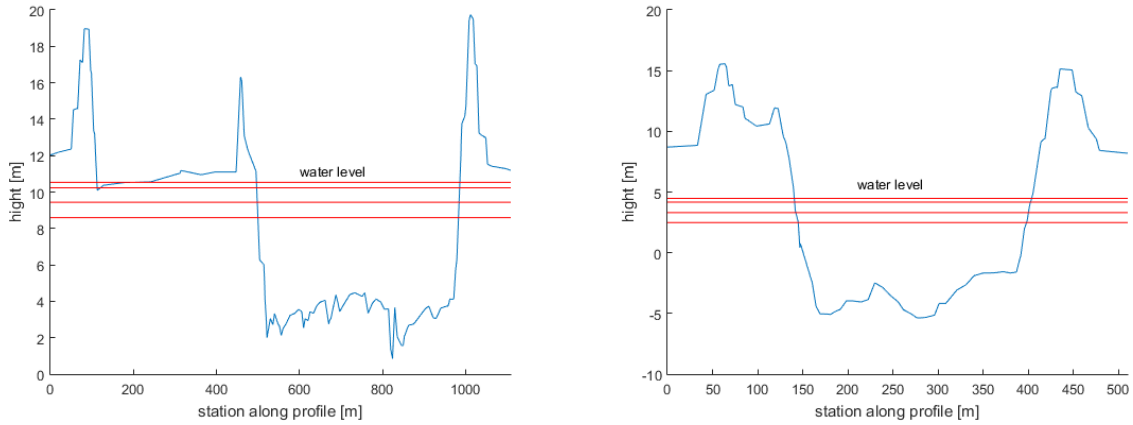

(a) *Sermide* ***(b)*** *Pontelagoscuro*

Figure 4.4: *River profiles; water levels through the year*

Table 4.1: *Profile widths 2001*

Season	Sermide	Pontelagoscuro
1	489.80 m	263.18 m
2	488.75 m	261.66 m
3	485.98 m	257.92 m
4	483.01 m	253.19 m

4.2 Classification Performances

The single classifiers are now represented in a bar chart with a color assigned to each of them (see Figure 4.5 and Figure 4.6). The red line shows the reference value from the in-field measurement.

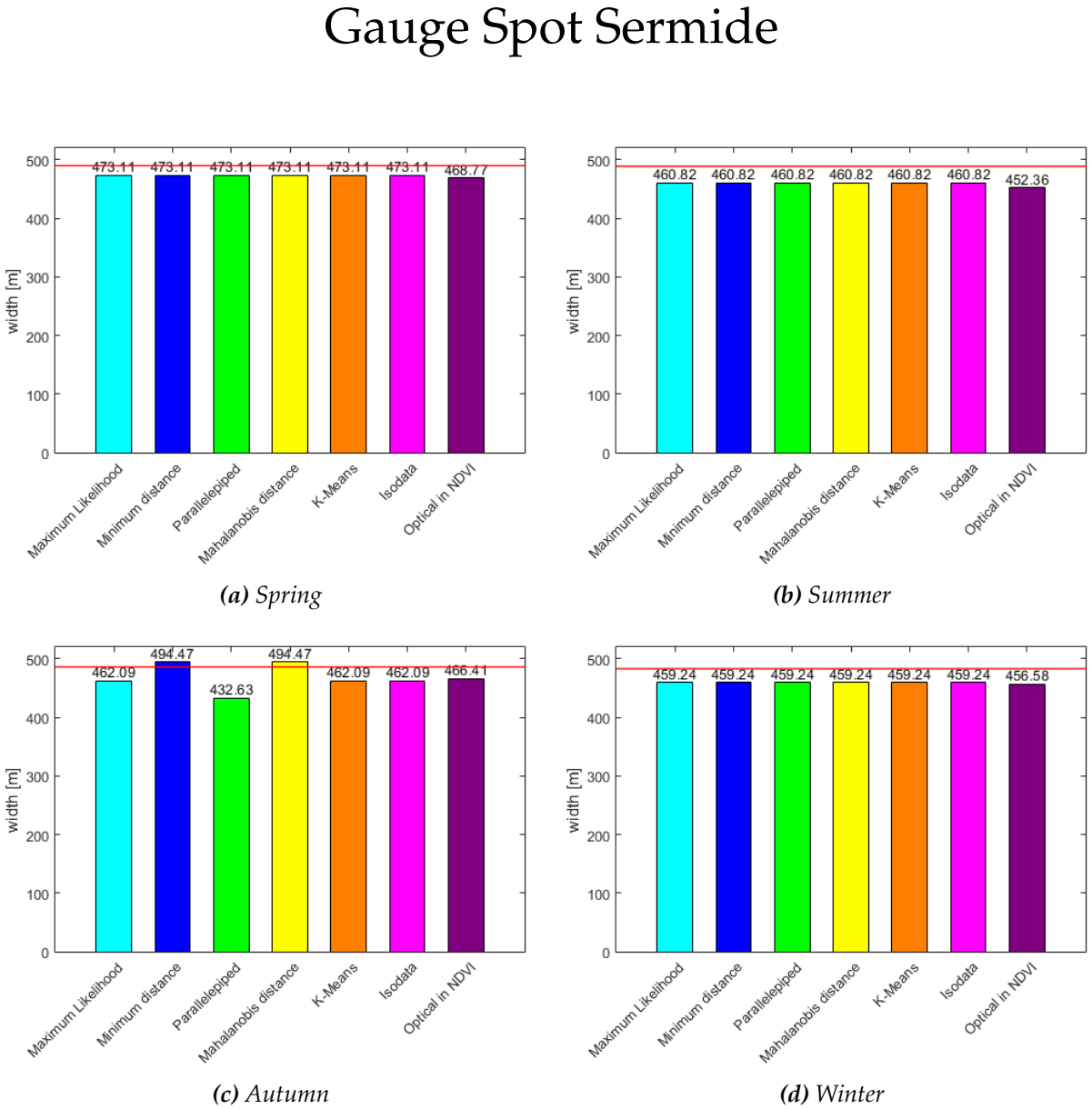

(a) *Spring* ***(b)*** *Summer*

(c) *Autumn* ***(d)*** *Winter*

Figure 4.5: *Classification performances in Sermide*

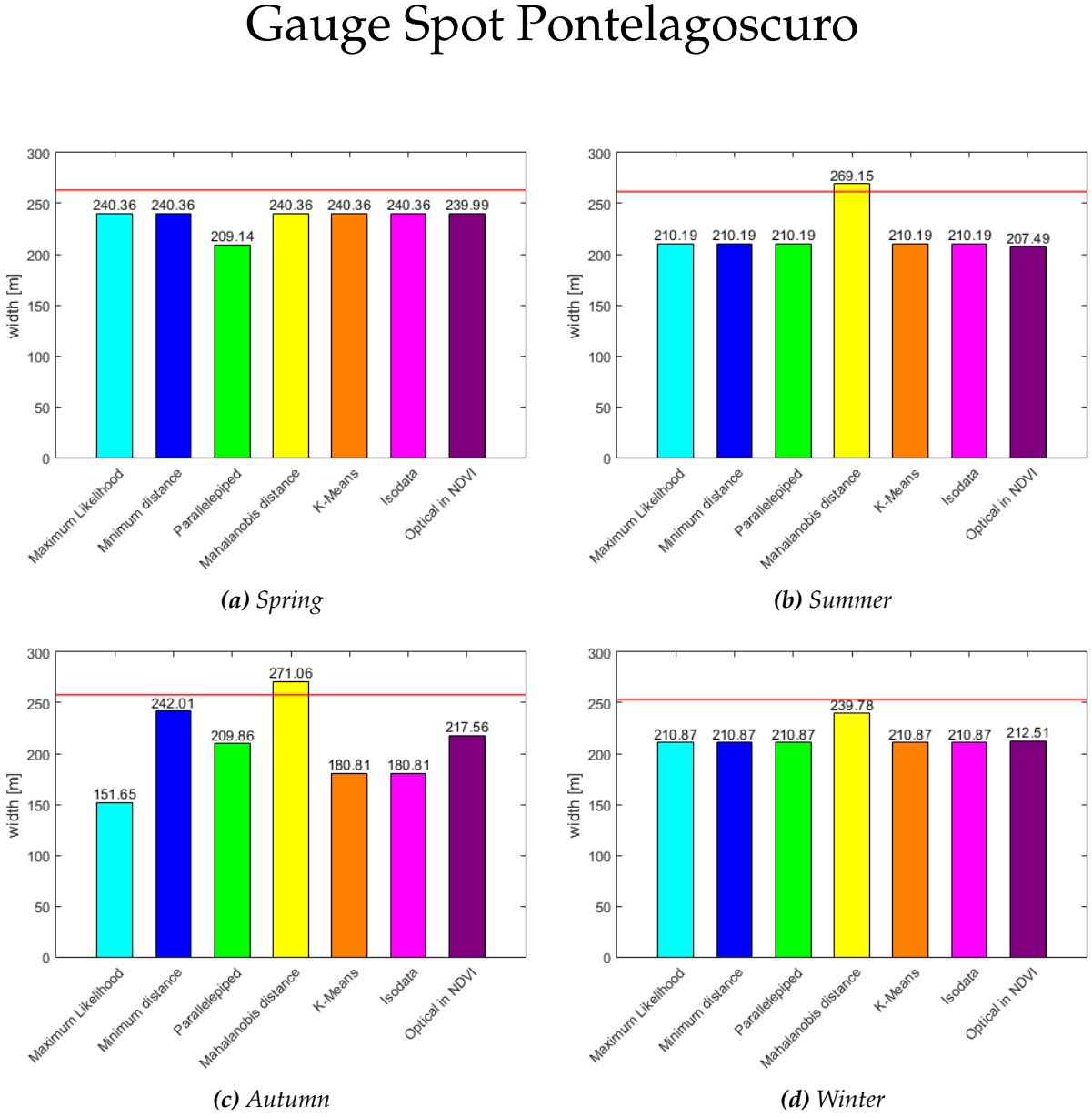

(a) Spring *(b) Summer*

(c) Autumn *(d) Winter*

Figure 4.6: *Classification performances in Pontelagoscuro*

Figure 4.7 shows the overall mean deviation from both measurement spots and all four seasons in percent and in Figure 4.8 the deviations were summarized to give an absolute value in the difference from the in-field measurement in metre.

In almost every case the classifiers assigned too little pixels to the river class resulting in much narrower widths compared to the in-field measurement. The Maximum likelihood along with the parallelepiped classifier show less performance. Not only they showed many misclassified pixels but also the profile measurements alongside the river were the least accurate. It has to be mentioned that the maximum likelihood classifier showed some very unlucky misclassification in Pontelagoscuro (Figure 4.6c) which is the main reason why it was so outperformed by the other classifiers in such a big manner. A few errors in the water class appeared but it was able to identify disruptive elements like clouds and shadows sharply.

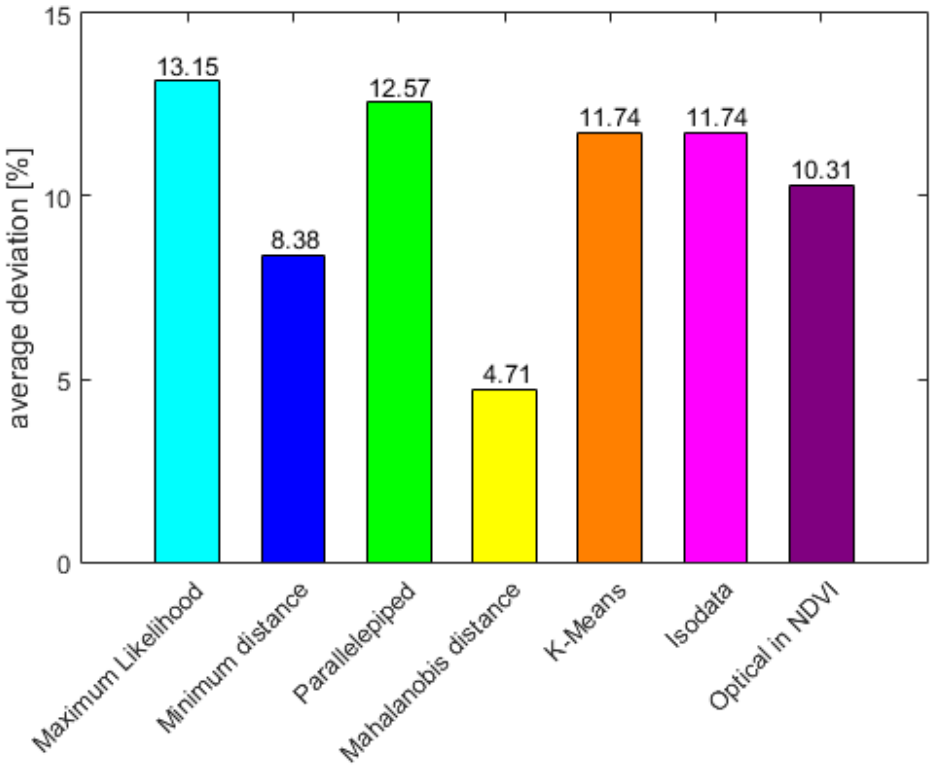

Figure 4.7: *Average percentaged deviation*

The parallelepiped classifier left many pixels as unclassified but still created very firm boundaries in between the classes and it was the only classifier which was able to clearly identify bridges and other small objects alongside the river. The unsupervised classification techniques performed slightly better than the parallelepiped classifier. They both performed equally well, there was no significant difference in the subset where the profile measurements were applied. In some other areas the images classified by Isodata clustering looked like an eroded version of the ones created with the k-means classification meaning the river was thinned out and as a result the boundaries appeared more accurate. When it comes to disruptive elements like shadows or brightness issues the unsupervised techniques did not perform very good. Same goes for the urban areas.

Close behind the accuracy of the remaining two classifiers it was advantageous to just measure the profile in a visual way with the help of the NDVI image. Of course it is very difficult to distinguish between water and land in a greyscale image with a spatial resolution of 30 m but still this method led to acceptable results.

The second best performance was approached by the minimum distance classification. It performed very good in cases of thin layers of water and also created very firm boundaries between the single classes. Like the unsupervised methods it had some issues in identifying urban areas but overall the misclassified areas are kept within a limit.

Among the classification methods used in this thesis we can see clearly that the mahalanobis distance classifier outperforms as far as the river widths are concerned. It often looks very

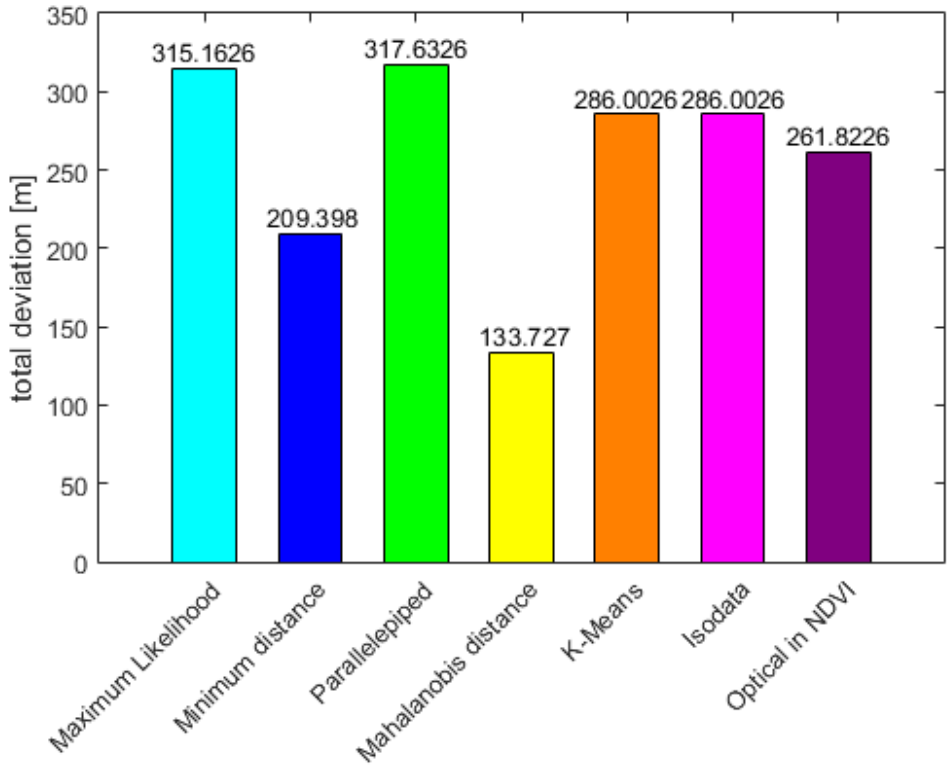

Figure 4.8: *Absolute deviation from all eight measurements*

pixelated and also a few errors in the coastal region and in distinguishing between wet soil and water appeared. However, it is by far the best classification method in the urban area and it also assigned pixels beneath clouds and in shadowed areas more accurate than any other classifier.

Chapter 5

Conclusion and Outlook

5.1 Conclusion

In this study the unsupervised clustering algorithms were outperformed by the supervised classifiers. But still these methods are suitable for quick and reliable results and create very firm boundaries in between the classes. Same goes for the comparatively simple algorithms like the parallelepiped and the maximum likelihood classification. Also a brief visual measurement in the NDVI or in a RGB image gives a good first overview of the local conditions. The best result is achieved by the minimum distance and the mahalanobis distance classifier. What both have in common is how they assign unknown pixels to a class: they both look for the smallest distance in spectral space.

However, it has to be noticed that these results only apply to the two gauge spots used for this study. A general statement about the mahalanobis distance classification being the best method among the six classifiers can not be made. Depending on different environmental circumstances other classifiers may lead to better results. On individual applications one should always test different classification methods to see which one gives the most reliable results.

5.2 Outlook

One of the most crucial points for reliable remote sensing image analysis is the spatial resolution. Landsats relatively low resolution of 30 m implemented on a 300 m wide river profile does not leave vast room for interpretation. To guarantee more reliable results measurements on water surface areas instead of river profile widths could be applied. Area-wise comparison between the classification results and these so called *effective river widths* may lead to better estimates but such an arrangement would require good testing grounds alongside the observation area.

The extent of this bachelor thesis could not cover all issues of this topic. However, despite the low resolution, good first impressions of the advantages and disadvantages of a wide range of classification methods were given. It is a good starting point for further studies in this area of research.

Bibliography

[1] Elmi, O. [2015], The role of multispectral image transformations in change detection, Master's thesis, University of Stuttgart.

[2] EXELIS [2015], 'classification'.
URL: *http://www.exelisvis.com/docs/classification.html*

[3] GDSC [2015], 'band combinations'.
URL: *http://gdsc.nlr.nl/gdsc/en/information/earth_observation/band_combinations*

[4] *Landsat 7 Picture* [n.d.].
URL: *http://www.lockheedmartin.com/content/dam/lockheed/data/space/photo/landsat-7.jpg*

[5] NASA [2015*a*], 'Nasa landsat science'.
URL: *http://landsat.gsfc.nasa.gov/*

[6] NASA [2015*b*], 'The Landsat 7 summary'.
URL: *http://geo.arc.nasa.gov/sge/landsat/l7.html*

[7] *Resolutions of Remote Sensing* [n.d.].
URL: *http://www.edc.uri.edu/nrs/classes/nrs409/rs/lectures/howremotesensonwork.pdf*

[8] Richards, J. A. [2012], *Remote Sensing Digital Image Analysis - An Introduction*, 5. edn, Springer Science and Business Media.

[9] Schowengerdt, R. A. [2007], *Remote sensing: models and methods for image processing*, Academic Press, Oxford.

[10] Siegmund, A., Kollar, I. and Siegmund, A. [2015], 'Introduction to Remote Sensing'.
URL: *http://www.seos-project.eu/modules/remotesensing/remotesensing-c00-p02.html*

[11] Unsalan, C. and Boyer, K. L. [2011], *Multispectral Satellite Image Understanding - From Land Classification to Building and Road Detection*, Springer Science and Business Media, Berlin Heidelberg.

[12] U.S. Geological Survey [2015*a*], 'Landsat 8'.
URL: *http://landsat.usgs.gov/landsat8.php*

[13] U.S. Geological Survey [2015*b*], 'Slc-off products: Background'.
URL: *http://landsat.usgs.gov/products_slcoffbackground.php*